EFFUSION OF CHARGED PARTICLES FROM A SHOCK HEATED GAS

Thesis by

Bradford Sturtevant

In Partial Fulfillment of the Requirements

For the Degree of
Doctor of Philosophy

California Institute of Technology

Pasadena, California

1960

ACKNOWLEDGEMENTS

The author takes pleasure in thanking Dr. Hans Wolfgang Liepmann for his guidance and fruitful advice during the course of this work. The contributions of other members of the staff of the Guggenheim Aeronautics Laboratory are also gratefully acknowledged. Special thanks are due to Dr. Anatol Roshko for his help with the experimental techniques and Dr. Julian Cole for his contributions to the theoretical considerations.

It is a pleasure to thank Mrs. Dorothy Diamond and Mrs. Geraldine Krentler for their competent preparation of the figures and typescript.

The author is indebted to the Lockheed Aircraft Corporation and Douglas Aircraft Company for their financial assistance in the form of fellowships and to the Office of Naval Research for the support of the experimental program under contract N-onr 220-21.

ABSTRACT

An experimental and theoretical investigation is made of the application of a molecular beam type sampling device for studying low density shock tube flows to the case of slowly ionizing argon behind a reflected shock wave. The flux of charged particles from a gas heated to about $10,000^{\circ}K$ and 20 mm. Hg. through a small orifice in the shock tube end wall is measured. The processes determining this flux are the initial stages of ionization in argon and the diffusion of charged particles to a cold metallic wall. Providing the diffusion process is understood, the measurements constitute a direct observation of incipient ionization ($\alpha \sim 10^{-7}$).

The transient charge diffusion mechanism is studied in detail theoretically, avoiding the assumption of ambipolar diffusion. It is concluded that the major problem lies in the understanding of the wall-gas interaction as represented by boundary conditions at the wall. An approximate relation for charge effusion is derived.

It is concluded from the experimental results that the initial ionization can not be due to a single step, electron-atom collision process but must result from a series of several atom-atom collisions resulting in the ionization of argon atoms.

TABLE OF CONTENTS

TABLE OF CONTENTS (Con't)

TABLE OF CONTENTS (Con't)

1. Introduction

This paper is a description of a new method for studying low density high temperature shock tube flows. The motivation for developing new methods lies not only in the fact that most customary shock tube instrumentation (e.g. optics) is less sensitive at low densities but also that there exist well-known techniques in other fields of physics that are more indigenous to low densities and high temperatures. Notable among these is the class of "beam techniques" which utilize low and high energy beams of molecules, atoms, and electrons for such studies as mass spectroscopy, nuclear resonance, etc.

The present experiment uses the shock tube as a conventional "source" for a molecular beam which is expanded to very low densities through a small orifice in the wall of the tube. The study of the properties of the beam downstream of the orifice with conventional molecular beam techniques can be used to obtain information about the processes taking place in the shock tube itself. In effect, small samples of gas are removed from the shock tube and studied.

The removal of gas through the orifice depends on the flux of mass toward the wall from the shock heated gas. This situation is analogous to the familiar shock tube heat transfer techniques which measure flux of heat to the "wall". The one measurement involves diffusion of mass, the other diffusion of heat. Since both involve transport processes in the gas it is evident that they will be very closely coupled. In fact, the measurement of mass diffusion to a wall

or body represents an independent observation of transport processes which may be particularly useful in experiments with multi-component gases, chemical reactions, etc.

The analogy between heat transfer experiments and this mass transfer experiment can be used to clarify the point of view taken here. With both techniques there are two possible uses of the experimental data; either a) the experiment and a heat or mass transfer theory are used to obtain information about the nature of the shock tube flow far away from the wall, or b) the experiment and known conditions at "infinity" are used to obtain information about the heat or mass transfer theory. Of course both the heat and mass transfer theories are included in the complete Navier-Stokes equations appropriate to the experimental configuration.

If the temperature of a thin film heat transfer gauge is very nearly that of the surrounding wall, then the heat transfer to the film is the same as to the wall. Similarly, if the amount of mass removed through the hole is very small (i.e. if the hole is very small), then the hole does not affect the surroundings, and the flux to the hole is the same as to the wall. This is classical Knudsen effusion and is the case considered here.

The purpose of the present experiment is to demonstrate the utility of the technique by applying it to a well-suited but simple experimental and theoretical problem. The configuration chosen is illustrated in figures 1 and 2. The hole is placed in the end wall of the tube with the result that the relatively stagnant gas heated by the reflected shock effuses through the orifice. Just as the heat transfer to the end wall is the simplest shock tube heat transfer problem so is the mass

transfer to the end wall. Since the enthalpy behind a reflected shock of moderate strength is sufficient to partially ionize a monatomic gas and since an electric current is one of the easiest things to measure, it was decided to measure the effusion of electrically charged particles from shock heated argon by collecting the particles on electrodes downstream of the hole. The mass transfer process involved in this measurement is the diffusion of electrons and ions to the wall and the conditions at "infinity" are determined by the ionization relaxation process.

In the execution and interpretation of this experiment many of the problems that arise are interesting in their own right. For this reason some are treated in greater detail than required for the immediate purpose of this program. Others are considered only insofar as necessary to define the experiment. The major problems discussed in the following sections are summarized below:

1) Shock tube performance at low pressures. It has been found that the departure of shock tube performance from idealized shock tube theory increases as the operating pressure decreases. Indications of the nature of the departure in the region near the end wall are obtained by conducting calibrating experiments over a large range of conditions from high pressures where shock tube performance is well understood to pressures typical of the charged particle effusion experiments.

2). The effusion of a neutral gas from a source in which temperature and density gradients exist. The usual analysis for Knudsen effusion assumes isothermal equilibrium, while the transient (non-equilibrium) processes in the shock tube support thermal gradients. This problem can be handled with an accuracy sufficient

for present purposes by using simple diffusion theory (Sec. 3.1).

3) The diffusion of charged particles from a hot gas to a cold wall. Problems associated with the interactions of hot gases with cold bodies are becoming more numerous and important as time goes on. Shock tube heat transfer experiments in un-ionized gases represent a phase of this problem already extensively studied. The next step in difficulty occurs with monatomic gases at temperatures where the real gas effect is so slight that the non-electrical properties of the gas are only slightly affected. In this case, the charged particles are acted upon by electric body forces. The electric fields that appear are caused by the separation of charge and are therefore intimately connected with charge diffusion. This is the situation to which the customary electron and ion binary diffusion equations (usually written for constant temperature) apply. The coupling of the diffusion with such processes as flow over a body is so complex that even the simple continuum probe problem is not understood.

The present experimental configuration represents the simplest case for diffusion from a slightly ionized gas to a cold wall (Fig. 3) and has therefore been studied theoretically in some detail. The simplifying features are the following: the problem is one dimensional, convective velocities play a small role, no currents are drawn from gas to wall, there are no sources or sinks of charge except at the wall or at "infinity", and well-defined experimental conditions for continuum diffusion of charged particles exist. These simplifications permit an analysis in which the major features of the general diffusion process can be illustrated.

An important limiting case for the understanding of the

transient diffusion process is the steady state case (in particular, isothermal equilibrum between a wall and an electron atmosphere). In such a case, the separation of charge due to physical processes at the wall produces all the interesting physical effects. On the other hand, it is customary in more complicated steady state problems or in the transient case to distort these effects by assuming electron density everywhere equal to ion density (ambipolar diffusion). In the present analysis, this assumption is avoided, thereby illustrating which effects it does or does not distort.

It is concluded that the largest gap in the understanding of charge diffusion is in the "boundary conditions" at the wall. The physics of the response of the wall to the gas and the interaction at the interface are crucial to a better understanding of the total process.

It is also shown that in such a transient process (and presumably also in steady dissipative processes such as the flat plate boundary layer or normal shock wave) the characteristic length for electric field perturbation into the gas is not the Debye length but a "boundary layer thickness" for <u>electron</u> diffusion, $\delta \sim \sqrt{D_{en}\, t}$.

4) Ionization relaxation in argon. Table I illustrates the conditions in the reflected shock region both at "infinity" and at the interface between wall and gas for a typical experiment. It is evident from a comparison of the parameters for equilibrium ionization and the parameters observed in an actual experiment at 20 μ seconds that the experiments take place in the early stages of ionization. The nature of the reaction mechanism for the early stages

has been the subject of some speculation recently in the attempt to explain measurements of the approach to equilibrium (i.e. the late stages of ionization). The effusion experiment, since it is a direct observation of the early stages, can give some information on this problem providing the point of view is taken that the conditions at "infinity" are unknown and that the charge diffusion theory is sufficiently valid to be applied to the experimental data.

The analysis of the reaction kinetics in the initial stages is easier than in the later stages because the temperature, pressure and total density of the gas are constant. From a discussion of the properties of possible chemical reactions, a "local" empirical relation is derived for describing the observed process in terms of four constants determined from experiment. These constants fix the time behavior, pressure behavior, pre-exponential temperature behavior and total activation energy of the reactions observed. The experiments indicate that the portion of the process observed is indeed very slow and is equivalent to a series of six consecutive reactions. The total activation energy is very near the ionization energy of argon.

2. Shock Tube Performance at Low Pressures

The details of the shock tube design, instrumentation and calibration are presented in appendix I and are summarized in this section. Figure 1 schematically illustrates the apparatus, which is small and simple to facilitate the attainment of relatively high vacuua. The entire system has a leak rate of 5 microns per hour (measured with a McLeod gauge) from an ultimate pressure of about 10^{-5} m.m.

The permanent instrumentation consists of thin platinum heat

transfer films, amplifiers, and a microsecond counter for measuring shock velocity, and McLeod and Pirani gauges for pressure measurement. This instrumentation was used in preliminary experiments to determine the performance of the shock tube at the low design pressures. Measurements at low pressure of shock speed as a function of diaphragm pressure ratio, and shock attenuation and heat transfer as functions of Mach number are compared with the same measurements at high pressures, where the shock tube performance is very nearly ideal.

The two causes of departure from ideal behavior at low pressures in this shock tube are the relatively long shock formation distance (Ref. 4) and the shortening of shock wave - contact surface separation by boundary layer effects (Refs. 5, 6). The former makes itself evident in the film signals of figures 4 and 5 as a more gradual rise than the expected step function, in the increasing departure of shock speed from ideal as pressure decreases (Fig. 6), and in the increasing shock acceleration over two adjacent intervals with decreasing pressure (Fig. 7). That the contact surface gets closer to the shock as pressure decreases is illustrated by the early arrival of the re-reflected wave at the end wall in figure 4 and the early quenching of the side wall signals in figure 5.

The heat transfer data obtained from the film signals are plotted in figures 8 and 9. As can be seen in figures 4 and 5, the height of the initial step at high pressures is well defined despite the gradual subsequent rise on the side wall gauges due to their protrusion into the flow. However, at $p_1 = .1$ mm (Fig. 4c, 5c) the "knee" at the top of the initial rise has become so pronounced as to prevent an unambiguous determination of the step height, $\Delta E/E$.

The values plotted are taken at the base of the knee and therefore may be too low. This rounding at the top of the step is a common effect on thin film signals even at high pressures (Figs. 4a and 4b, gauge No. 4) and is not understood. Since it appears to be a function of pressure, it may indicate a non-ideal behavior of the temperature of the gas. This possibility is discussed in section 4.2 with respect to the ionization experiments.

3. Effusion from the Reflected Shock Region

In this section a detailed description of the mass transfer process is given in preparation for the discussion of the ionization sampling experiments. First the heat transfer and effusion process for a perfect gas is covered and then charge diffusion is added.

3.1 Effusion of a neutral gas. The reflected shock wave propagates away from the shock tube end wall leaving a hot stagnant body of gas. Its effect on the gas can be idealized by hypothesizing the instantaneous heating at time $t = 0$ of a semi-infinite body of compressible gas ($x > 0$) in contact with a semi-infinite wall ($x < 0$) at room temperature. The heating by the shock serves as initial conditions and boundary conditions at $x = \infty$ for the computation of the response of the gas and wall. This computation has been carried through in detail by Roshko in reference 7 under the assumptions that velocities due to mass displacement in the thermal layer can be neglected (constant pressure) and $K_n \sim T$ where K_n is the local heat conductivity and T local temperature. With the latter assumption the Howarth transformation can be used, resulting in a "locally" incompressible solution i.e. a solution which looks like the incompressible result but with transport parameters evaluated at

local conditions. At the wall and at $x = \infty$ where the temperature and pressure are known the solution is given by the well-known error function evaluated at the appropriate conditions

$$\frac{T}{T_w} = 1 + \frac{T_\infty - T_w}{T_w} \quad \text{erf} \quad \frac{x}{2\sqrt{\nu t/Pr}} \tag{1}$$

where T_w is the temperature at the interface, ν the kinematic viscosity and Pr the constant Prandtl number. The "thermal layer" given by this result has a thickness

$$\delta = \frac{2}{\sqrt{\pi\, Pr}} \quad \sqrt{\nu t} \tag{2}$$

The gas near the wall, where the density is very high (ν very small), "sees" a thermal layer much thinner than the gas at $x = \infty$.

Effusion from the reflected shock region can be computed using these results if the perturbation by the hole is small. The nature of effusion from a region of time dependent gradients is easily illustrated using the concepts of simple diffusion theory. A fundamental result from the kinetic theory of gases is that the flux of molecules in one direction across unit area of any plane in the gas (say, to the left across a plane perpendicular to the x-axis at $x = 0$) is

$$F_1 = - \frac{\eta(x = \Lambda_n)\ \bar{c}\ (x = \Lambda_n)}{4} \tag{3}$$

where the number density η and the mean thermal velocity $\bar{c}$ are to be evaluated at the average point of last collision, i.e. at $x = \Lambda_n$, the mean free path of neutral atoms. This result is customarily used to derive a first approximation to the net flux when conditions at $x = +\Lambda_n$ are different than at $x = -\Lambda_n$. A Taylor series expansion of the net flux leads to the familiar expression for diffusion,

$$F = \frac{(\eta \bar{c})_{-\Lambda_n}}{4} - \frac{(\eta \bar{c})_{+\Lambda_n}}{4} \doteq -\frac{\Lambda_n}{2}\left(\frac{\partial \eta \bar{c}}{\partial x}\right)_0 = -\frac{\Lambda_n \bar{c}}{2}\frac{\partial \eta}{\partial x} - \frac{\Lambda_n \eta}{2}\frac{\partial \bar{c}}{\partial x}$$

which constitutes a crude approximation to both ordinary and thermal diffusion. Thus equation 3 is useful even if gradients exist in the gas and can just as well be applied to the effusion of a gas through a small hole from the reflected shock region. If the density downstream of the hole is much smaller than upstream, the flux is in one direction and is given by equation 3. A Taylor series expansion for moderate gradients (i.e. for $\Lambda_n\left(\frac{\partial \eta}{\partial x}/\eta + \frac{\partial \bar{c}}{\partial x}/\bar{c}\right) \ll 1$) leads to

$$F = -\frac{\eta(x=0)\,\bar{c}\,(x=0)}{4} \tag{4}$$

The validity of this approximate result is closely related to the validity of the representation of the shock reflection process as the instantaneous heating of a semi-infinite body of gas. The latter idealization is evidently only valid if the shock is many shock thicknesses (mean free paths) from the wall, i.e. at times t such that $t \gg \tau_n$, where τ_n is the collision mean free time for atoms in the shock heated gas. Substituting this inequality into equation 2 then gives $\delta \gg \Lambda_n$ which is essentially the same as the inequality before equation 4. Therefore, the latter equation can be

used any time the heat transfer model is valid.

The above analysis emphasizes that effusion through a small hole is indeed a process of mass diffusion. The only distinction made here between effusion and diffusion is that effusion refers to the flux in one direction across a plane while diffusion refers to the difference between fluxes to right and to left. Thus, in general, if a gas is diffusing to a wall, the effusive flux through a hole is not the same as the net diffusive flux.

It is important to note that since, by equation 3, the particles effuse from the region $x \doteq \Lambda_n$ and since $\delta \gg \Lambda_n$, the mean energy of the beam is given by the wall temperature, i.e. 1/40 e.v. (Sec. V.2).

3.2 Charge diffusion. If the effect of the ions and electrons on the non-electrical properties of the gas is small, then their diffusion and effusion can be superimposed on that of the neutral gas. This decoupling of charge diffusion from heat transfer for small charge concentrations is illustrated in appendix II where the equations (II. 28) are derived in detail from the complete set of Navier Stokes equations with diffusion and Maxwell's equations. The model representing the ionization by the reflected shock is the same as that used above for the heat transfer: At time $t = 0$ the semi-infinite body of gas ($x \succ 0$) is heated and ionized to the given ion and electron number density $n_i (x = \infty) = n_e(x = \infty) \equiv n_\infty$ (Fig. 3, non-dimensional notation defined in Eq's. II. 19), n_∞ constitutes the initial condition and boundary condition at $x = \infty$ on the degree of ionization and, for the purposes of analysis, is taken as uniform and constant in time. The generalization to a charge density changing with time ($n_\infty(t)$) such as in the observed relaxation process is carried out later.

It is assumed that there are no chemical reactions in the gas except possibly at the wall or outside the diffusion layer (represented by $n_\infty(t)$). Equations appropriate to "frozen reactions" are considered in which the degree of ionization α appears explicity as an unknown (in contrast to equilibrium flow where the law of mass action gives $\alpha(p, T)$). In general, this presents the possibility of transport of energy by mass diffusion down concentration gradients in the absence of temperature gradients. However, since for small α heat transfer and diffusion are uncoupled, this effect does not appear in slightly ionized gases. A discussion of recombination in the cool thermal layer appears in Sec. V. 2.

To simplify the discussion, the further assumption is made that the flux of charged particles to the wall can be obtained by solving the diffusion equations for constant temperature and density (Eq's. II. 29) and computing the flux using the temperature and density at $x = 0$ as given by the third of equations II. 28. This can be considered as the first step of an iteration on the complete set of equations II. 28.

3.3 Boundary conditions. The major problem that arises in the analysis is the nature of the interaction between the wall and the gas (Appendix III). In general, the charge concentration and fields in the gas induce charge concentrations and fields in the wall as determined by the properties of the wall. At the interface appropriate matching conditions must be established between the responses of the gas and of the wall. It is possible to represent the response of the wall and the matching conditions as an effective boundary condition at $x = 0$ in the case of a metallic wall, since, by the free electron theory of metals, the effect of a change of charge distribution in the gas appears

almost instantaneously as a change of charge distribution at the interface. The wall acts like one plate of a plane condenser on which there is a charge concentration equal and opposite to the integral from $x = 0$ to ∞ of the gas charge density. For the case of diffusion to a "cold wall" (Sec. III. 3) the charge sheet consists of electrons. The field jumps from zero in the wall to a negative value $E(0, t)$ at the interface.

Another boundary condition required for equations II. 29 involves the flux of charged particles to and from the wall. This is perhaps the least understood aspect of the diffusion process. A cold metallic wall is strongly catalytic to recombination in the sense that it acts as a massive third body and an infinite reservoir of electrons (due to the electron sheet; section III. 3. 1). Because of this it is usually argued that there will be no charged particles left in the neighborhood of the wall and the boundary condition $n_e(0, t) = n_i(0, t) = 0$ (Eq. IV. 1) is used. In actual fact, the knowledge of the reaction at the wall only provides direct information on the fluxes to and from the wall and these can be related to the number densities by simple diffusion theory only under certain circumstances. A more accurate statement is simply that all ions reaching the wall recombine with electrons from the charge sheet. Thus in general there is a flux of ions to the wall but not from the wall, while there is a flux of electrons both to and from the wall (the latter by thermionic and photoelectric emission). Using equation 4 it can be said that for $\frac{\Lambda_{e,i}}{n_{e,i}} \frac{\partial n_{e,i}}{\partial x} \ll 1$ (i. e. near equilibrium) the flux in either direction across a plane approximately defines the number density at the plane (c. f. early references on equilibrium summarized by Fowler, Ref. 8)

$$n_{e,\,i}(0) = \frac{4\,F_{e,\,i}(0)}{\bar{c}_{e,\,i}} \tag{5}$$

However, for such small $n_{e,\,i}$ that the inequality doesn't hold, there is no equivalent equation for $n_{e,\,i}(0)$. Thus $n_e(0) = n_i(0) = 0$ cannot be justified by a recombination argument.

It can furthermore be shown (Sec. IV. 2) that this boundary condition is necessarily inapplicable for large times since it inevitably leads to arbitrarily large electric fields. This is because the body force terms in equations II. 29 do not contribute to the flux to the wall and the electrons are not inhibited from diffusing to the wall in larger numbers than ions. By equation II. 27 this causes a continually negatively growing field.

In section IV. 3 it is shown that for times much larger than τ (the time for an electron to diffuse one Debye length; Eq. II. 19) the electrons are, to a first approximation, in equilibrium and therefore, to the same approximation, equation 5 can be used to set the boundary condition $n_e(0)$. The flux $F_e(0)$ is given by thermionic or photoelectric emission, whichever is appropriate. The resulting matching condition leads to a finite number density $n_e(0)$, a finite field at the wall and a steady wall potential of about 1 volt. However, for the particular numerical values appropriate to the present experiments, the calculated result $n_e(0)$ (Sec. IV. 3. 1) is smaller than the inaccuracy in the calculation (i. e. the extent of electron equilibrium). If

$$n_e(0) = n_e(0)_{\text{calculated}} \pm \Delta n_e(0)$$

then it turns out

$$n_e(0)_{\text{calculated}} \ll \Delta n_e(0)$$

Thus the best conclusion that can be made is

$$0 < n_e(0) \leq \Delta n_e(0)$$

or, in non-dimensional notation

$$0 < n(0) \leq O(D) \tag{6}$$

where D is the square root of the ratio of electron mass to atom mass.

The boundary condition $n_i(0)$ is still undetermined but, since $n_e(0) \neq 0$ insures reasonable electron diffusion and finite fields, it seems consistent to retain the approximation $n_i(0) = 0$.

From the equations for large time, the further important and familiar result is derived in section IV. 3. 1 that, to a first approximation, the ion diffusion to the wall is unperturbed by the electric body forces. Within the accuracy of a first approximation, the ambipolar diffusion result II. 37 or "independent" diffusion result IV. 5 give equally valid results for ion fluxes. This not only provides a means of calculating n_∞ from an observed flux but emphasizes the fact that the non-linearity of the body force terms in equations II. 29 is weak. The approximate ambipolar or independent diffusion results are solutions to linear equations and can be superposed to give a solution for the general boundary condition $n_\infty(\infty, t)$. This is carried out in section V. 2.

For $n_i(0) = 0$ the body force terms in equations II. 29 do not contribute to the net diffusive flux at the wall so

$$F_i(0) = \left(D_{in} \frac{\partial n_i}{\partial x}\right)_o \tag{7}$$

It is pointed out before equation 5 that since the wall is a perfect sink of ions there is no flux of ions from the wall to the gas. The net diffusive flux is therefore identical to the flux to the wall. If conditions V. 7 are fulfilled, then the hole does not disturb the charge diffusion and the flux to the wall is the same as through the hole. Therefore the quantity $n_{\infty}(t)$ is related to the experimentally measured effusive flux of ions $F_i(0, t)$ by the approximate result of the superposition, equation V. 6.

3.4 Summary. The conditions exhibited in Table I for a typical experiment illustrate the general nature of the charge diffusion process represented by equations II. 29. At $t \approx 20$ μseconds the thermal layer is many mean free paths thick so charged particles suffer many collisions as they pass through the thermal layer toward the wall. The characteristic distance from the wall for a measurable perturbation in electric field (i.e. a non-dimensional field E* of O (1); c.f. last paragraph App. IV) is not the Debye length as in the equilibrium case but is the electron boundary layer thickness $\delta_e \sim \sqrt{D_{en}\, t}$ which is much larger than the thermal layer thickness

$$\frac{\delta_e}{\delta} = \sqrt{\frac{1}{D}} \sim 16$$

It can be said that the large body forces required to set up ambipolar diffusion are generated by free electron diffusion outside of the main ion diffusion layer.

The Debye length, which is much smaller than the thermal layer thickness, represents the decay distance from the wall for the effect on the field of surface inhomogeneities such as roughness or atomic adsorption or the presence of a hole causing local field perturbations.

The mean free path does not enter in the discussion of the diffusion process which is a continuum process but only in the determination of the effusion through the hole which depends on the familiar simple kinetic theory argument. The inequalities V.7 state the conditions under which the hole will not greatly perturb the body forces or the effusion process. These conditions are not met in the present experiments. However, from the discussion of experimental results in section VI.2.2 it is concluded that the use of equation V.6 nevertheless represents a valid approximation.

The convenient length for non-dimensionalization in dissipative and equilibrium processes is the Debye length since the Poisson equation enters in both. In the dissipative process the characteristic time τ is the time required for an electron to <u>diffuse</u> one Debye length. Compare this with the period of a plasma oscillation which is the time for an electron to "fly" with mean thermal velocity one Debye length.

$$\tau = \frac{\lambda_\infty^2}{(D_{en})_\infty}$$

$$\frac{1}{\omega_p} = \frac{\lambda_\infty}{\bar{c}_{e\ \infty}}$$

It is evident that the former is characteristic of a process in which the mean free path is smaller than a typical length (say the dimension of a container or the thermal layer thickness or the Debye length itself) while the latter is typical for long mean free paths.

4. Ionization Theory and Experiments

The experimental apparatus for measuring the effusion of charged particles through a small orifice is illustrated in figure 2 and described in detail in section VI. 1. The ions are collected on a negatively biased electrode and the electrons on a positive electrode, both situated just downstream of the hole. The biases are large enough so that most of the effusing charged particles are collected but are small enough that secondary electron production at the ion collector is negligible. Experiments were carried out measuring ion current as a function of time with the instrumentation indicated in figure 2 over a small range of Mach numbers and initial pressures with different "impurities" added.

4. 1 Preliminary experiments. In this section the characteristics of the experimental measurements and the effect of "impurity" addition are indicated qualitatively. Figure 10 illustrates typical oscilloscope records at three different pressures in which the upper trace records the ion current and the lower trace indicates the response from the end wall gauge. The traces in figure 10a illustrate the whole process with the initial rise in ion current due to the ionization process, the subsequent quenching due to recombination in the growing thermal layer (Sec. VI. 2. 2) and the beginning and end of the run as indicated by the heat transfer gauge in the reflection of the wave from the end wall and the arrival of the re-reflected wave, respectively.

Figure 11 indicates the effect of the addition of "impurities" into the shock tube. Mercury at about 25 microns pressure was introduced by heating the tube with heating tapes and heating an

adjoining test tube of liquid mercury with a candle. A comparison of figures 11a and 11b indicates that the ionization level is greatly increased by the mercury. Figure 11c illustrates the whole process in the same way as figure 10a but with a sensitivity 1000 times less. Figure 11c shows a degree of ionization much nearer to equilibrium than that observed in 10a and emphasizes the "slowness" of the ionization process discussed further below.

Figure 11d illustrates a typical run in which the initial pressure was 95 μ of argon plus 5 μ air. Data were taken from such runs in the same way as described below for pure argon. The ion current at 20 μ seconds after shock reflection when plotted with the data of figure 13 for pure argon falls on the 100 μ curve with the same scatter as shown in the figure. Thus small amounts of added air do not cause large effects in the ion current. Increasing amounts of added air have no effect until the effect of the changing ratio of specific heats, γ , reduces the temperature in the reflected shock region and consequently in the ionization level. At no time does added air give ion currents larger than those observed in the purest argon.

4.2 Experimental results. The discussion in section V.3 of the properties of chemical reactions that will hold in general for the initial stages of ionization (where only atom-atom forward-going reactions are important in the production of electrons) suggests a local empirical representation of the functional dependencies of the process,

$$n_\infty = \eta_\infty^{\,q}\, T_\infty^{\,r}\, t^s \exp(-E_+/k\,T_\infty) \qquad (8)$$

where s depends on the number of consecutive reactions taking place at a given time, q depends on the binary nature of the collisions and the number of consecutive reactions, r represents the pre-exponential temperature dependence resulting from integrating over the velocity distribution, and E_+ in the familiar Boltzmann factor is the total activation energy for the process at a given time. Using equation V.6 to relate the charge density n_∞ with the observed ion flux gives

$$F_i(0) = \eta_\infty^{q'} T_\infty^{r'} t^{s'} \exp(-E_+/k T_\infty) \tag{9}$$

where $q' = q - 1/2$, $r' = r - 1/2$, $s' = s - 1/2$.

Two bits of information are obtained from each trace such as figure 10b or 10c; the numerical value of ion current at 20 μseconds after shock reflection and the time behavior of the current as obtained from a replot of the trace on log-log graph paper. From equation 9 the latter gives

$$\frac{\partial \ln F_i}{\partial \ln t} = s' \tag{10}$$

This result is plotted in figure 12. The pressure and Mach number dependency is largely due to the effects of recombination in the cool, dense thermal layer which are larger at high pressure and Mach number. The effect of recombination is estimated to be 1 per cent at $p_1 = 60\,\mu$ and $M = 6.5$ (Eq. V.13). It is concluded that for the conditions of this experiment s' is 6 and therefore s is at least 6. The part of the process that this experiment records can be represented empirically as a set of six consecutive reactions. This result emphasizes the evident complicated nature of the process. The most complicated

process proposed in detail to date is Weymann's two consecutive reaction process (Ref. 9). The above result seems to indicate an even more intricate process.

It is evident that accurate determination of the origin of time in the process (i.e. time of shock reflection) is very important in relaxation experiments. In these experiments the time of flight of the particles from the gas to the collectors is minimized by locating the collectors just downstream of the hole. The uncertainty in time origin due to time of flight and shock reflection time can be no more than 2 μ seconds. However, if the rounding of the end wall thin film signal mentioned in section 2 above and graphically illustrated in figure 10 where the time scales are greatly enlarged over the usual case is interpreted as a non-ideal temperature behavior outside the thermal layer, then an uncertainty is introduced in an effective time origin of at least a few microseconds.

The only other relaxation experiments in which the shock location has been illustrated simultaneously with a quantitative indication of electron density are the interferometric studies of Alpher and White (Ref. 10) of the region behind a strong incident shock in argon. Though run under radically different experimental conditions than the present experiments the occurrence in high purity experiments (Fig. 3, Ref. 6) of a long distance behind the shock with no observable relaxation followed by a very sharp rise to equilibrium lends support to the observation in the present experiments of a very slow process in the initial stages.

The second bit of information obtained from the traces is the ion current at 20 μ seconds after shock reflection (Fig. 13). Recombination

in the thermal layer at high pressures and Mach numbers depresses the value of ion current and is evident in this figure in the crowding together of the data and the decrease of slope as pressure increases. Since the effect of recombination in the thermal layer is least at low pressures and is computed to be 1 per cent at 60 microns the data at this pressure can be used with equation 9. The slope of the dotted line through the data is, from equation 9,

$$\frac{\partial \ln F_i}{\partial 1/k T_\infty} = -(E_+ + r' k T_\infty) \qquad (11)$$

and from figure 13 is equal to -12.6. r' is not known here but is usually negative, so it is concluded that for the conditions of these experiments E_+ is at least 12.6 electron volts.

An arbitrary generalization of Weymann's two consecutive reaction process to an s consecutive reaction process (Eq. VI.2) and the use of the value $s = 6$ determined above fixes a local value of $r' \doteq -3$. Substitution of this into equation 11 leads to $E_+ \sim 15.6$ volts. This value is very close to the argon ionization potential of 15.76 volts. Thus the data in figure 13 indicate that the major source of electrons and ions in these experiments is argon atoms.

APPENDIX I

SHOCK TUBE DESIGN, INSTRUMENTATION AND CALIBRATION

I.1 Design

Table I indicates the conditions for which the shock tube was designed. The primary objective was the attainment of vacua which would permit experiments in fairly pure argon at initial pressures less than 100 microns Hg. This was achieved by keeping the system (Fig. 1) as small and simple as possible. Since p_4 is always so low that the final pressure after a run is less than atmospheric, simple fittings and standard glassware could be used. The shock tube and driver sections are made of 3 in I. D. x 1/4 wall stainless steel seamless tubing with welded 3/8 inch flanges grooved for O-rings, and the beam section is a 1 foot length of 6 in. I. D. Pyrex Double Tough pipe with standard flanges and grooves to which O-rings are fitted. The entire system is tied to a foundation by the 1/2 in. thick stainless steel plate separating the shock tube and beam sections. As shown in figure 1 a cone is machined from this plate about the axis of the shock tube tapering from a 4 in. diameter to a 1/16 diameter hole at the axis. A small .001 or .002 in. steel diaphragm through which is drilled the hole that connects the shock tube with the beam section is fixed over the 1/16 hole with Apiezon black wax.

Connected to the beam section through a CEC two inch throttling gate valve and a special design stainless steel high conductance liquid nitrogen trap is the VMF 50 oil diffusion pump. The

limiting factor in pumping the shock tube is the five foot long piece of 16 mm. glass tubing connecting it to the beam section. The valves for selecting the mechanical pump function (roughing or backing) and for closing the 16 mm. connecting tubing are 10 mm. glass stopcocks. The lines from the mechanical pump (Cenco Hypervac 20) to the first stopcock and from the stopcock to the diffusion pump (through a 6 in. dia x 2 ft. long fore volume) are 5/8 inch I. D. rubber vacuum tubing. With the forevolume, the system can be pumped at ultimate pressure without the mechanical pump for more than 1/2 hour before the fore pressure gets so high that the diffusion pump loses efficiency.

All glass to metal seals are made with quick disconnect vacuum fittings of Veeco design, and removable glass to glass seals are of standard taper interchangeable ground glass joints.

Two types of diaphragm are sufficient to give bursting pressures from zero to over 3 atm. abs.; .003 cooper shim stock (1/4 hard) for pressures of less than 1 atm. abs. and .006 dead soft aluminum foil for high pressures. The breaking pressure is controlled by the depth of a Y-shaped scribe in the diaphragm. A hand driven puncturing mechanism was provided in the driver section but was seldom used since the scribing technique was found to give sufficiently repeatable bursting pressures.

The shock tube and driver sections are clamped together(with a diaphragm between) by small C-clamps so that the used diaphragm can be removed and the new inserted with a minimum of delay. After a run the shock tube is filled to atmospheric pressure with argon, the diaphragm is changed and the system is rough pumped immediately,

having been exposed to atmospheric air less than one minute. The time to pump from atmospheric to 3 microns Hg is 3 minutes. In a typical run the system is evacuated for about 10 minutes to less than .1 micron, flushed with argon to a few mm. and then re-evacuated to the experimental pressure of 100 microns or less. The stopcock separating beam and tube sections is then closed and the beam section becomes evacuated in a few seconds giving a pressure ratio across the hole of about 500. The time required to make a complete cycle from one run to the next is about 20 minutes.

The leak rate of the entire system is about 5 microns per hour. From this a crude estimate of the amount of "impurities" (most of which is probably air) can be made. For a typical initial pressure p_1 of 100 microns the leak rate is 5 per cent per hr. The amount of time that elapses between the flushing of the tube and breaking of the diaphragm is usually about 3 minutes, so the amount of air in the argon is certainly less than 1/4 per cent. The effect of impurities on the ionization process is discussed in section VI. 2. 3.

I. 2 Permanent Instrumentation

The permanent instrumentation consists of 1) pressure gauges, 2) shock speed measuring devices, and 3) an oscilloscope. A mercury McLeod gauge is used for making absolute measurements of pressures from .01 to 200 microns while continuous readings in the same range are made with a temperature compensated Pirani (hot wire) gauge calibrated from the McLeod gauge. The Pirani tube and dummy compensator form one side of a ten to one bridge and are heated at 20 ma. by a 6 volt storage battery. Both tubes are packed in fibre glass in a reflecting container to further minimize effects of ambient temperature changes.

Customarily the bridge is balanced at a given pressure (e.g. 100 μ) as measured by the McLeod gauge and for all subsequent runs at that pressure the system is merely pumped until the bridge is rebalanced. For pressures above 200 microns a Wallace and Tiernan absolute pressure manometer is used.

The transducers for measuring shock velocity are standard thin platinum resistance films evaporated and baked onto Pyrex glass backing and mounted in the shock tube in 1/2 in. dia. plugs 10 inches apart as shown in figure 1. The films are roughly 1/2 x 1/16 in. and usually measure between 50 and 100 ohms resistance after baking. The 1/2 x 1/8 in. backing material is cut from 2 mm. Pyrex plate. Leads are soldered to silver paint (du Pont No. 4760) fired to the back of the Pyrex plate and are lead out of the plugs through Carborundum covar-glass hermetic seals.

The films are heated with D.C. voltages of from 1 to 5 volts by separate 12 volt dry cell supplies. The films are therefore not operated at constant current and the data must be corrected for this. The signals from both films are fed to a single 3 x 5 x 7 inch unit consisting of 2 stages of transistor amplification with mercury cell supply, a ballast Helipot potentiometer, and a milliammeter for each film. The outputs from this unit go directly to the "start" and "stop" inputs of a Berkeley 7260 microsecond counter.

The oscilloscope used in the experiments is a Tektronix 551 dual beam with two 53/54 L preamplifiers coupled with two special 1000X gain low noise pre-preamplifiers designed by Mr. Richard Swartley, and mounted on the same scope mobile complete with separate power supply.

I. 3 Calibration

The purpose of the calibration was to determine the performance of the shock tube at low pressures ($p_1 \sim$ 100 microns). Because of the low operating pressures and short length of the tube (20 diameters) two possible deficiencies in performance might be expected; the shock may not be fully developed and the testing time might be very small.

The former would affect an experiment through the non-uniform conditions which would inevitably exist in the region behind the shock wave. This effect is minimized in the ionization experiments since the convection of these non-uniformities to the end wall is small. A measure of the departure of the shock from its fully developed state is obtained by comparing the speed of the shock with theoretical predictions (Section I. 3. 2) and by measuring its attenuation (Section I. 3. 3).

The testing time at a station on the side wall (Fig. 14) is given either by the time between the shock and contact surface, or the time between the shock and reflected shock, depending on station location and conditions in the flow. On the other hand, the end wall testing time is given by the time between shock reflection and arrival of the wave (a compression wave for strong shocks) which has been re-reflected from the contact surface. Both side and end wall testing times decrease as the contact surface gets closer to the shock wave. With a short tube the testing time obviously is small. Roshko (Ref. 5) has shown that, in addition, boundary layer effects at low pressures tend to decrease the distance between shock and contact, thereby decreasing the testing time. This effect was first reported by Duff (Ref. 6) and appears in the present experiments (Section I. 3. 1).

To observe these effects, the average Mach number over two adjacent 10 inch sections of tube and the heat transfer to side wall and end wall thin film resistance gauges were measured. The instrumentation used was that described in section I. 2 plus two additional films, another timer and another pre-preamplifier identical to the ones already mentioned. One of the films (44 Ω) was mounted in the same way as the permanent gauges (57 Ω and 58 Ω) on the side wall $21\frac{1}{2}$ inches upstream of the end wall, and the other (90 Ω) was evaporated onto Scotch splicing tape which was then stuck to the end wall of the tube. These gauges will be referred to below as numbers 1 to 4 depending on the order in which the shock hits them.

The signals from the films were amplified by the pre-preamplifiers and fed to the scope and the timers (the transistor amplifiers were not used). One timer was started by gauge No. 1 and stopped by No. 2 and the other timer was started by No. 2 and stopped by No. 3. The gauge signals were recorded by the dual scope in pairs. The qualitative nature of these signals is illustrated below and the numerical results of the measurements are presented and discussed.

I. 3. 1 Film signals. Figures 4 and 5 illustrate the typical behavior of side and end wall gauges. At 10 mm. the end gauge gives the predicted step function in temperature, but at lower pressures the signal becomes complicated by three effects: 1) The initial rise is more gradual than a true step, having a rise time of order 10 micro-seconds which is much longer than the thickness of an ideal normal shock. It would be expected that, since an incompletely developed shock wave is actually a train of waves of finite extent, the "thickness"

would be large. However, there are probably other factors that also contribute to this effect: a) In figure 11b there is shown to be a much slower rise at 60μ in mercury than in air and argon. Thus the shorting effect (next paragraph) contributes to the rise time. b) The nearness of the contact surface to the shock at these pressures also contributes to the complications at the wave front because it is possible for the diffusion thickness of the contact surface to be as large as the shock-contact surface separation. In fact, in the limit $p_1 \rightarrow 0$, the shock and contact surface are one and the same and diffusion determines the "shock"structure (c.f. Ref. 5).

2) At low pressures and high Mach numbers the ionization reaches the point where the characteristic resistance of the gas (defined in appendix VII) causes a significant decrease in the effective resistance of the film, i.e., a "shorting". In the most extreme case the effective resistance falls below the pre-shocked value and the scope trace falls sharply negative (Fig. 10c end gauge and Fig. 4a wall gauge). Under other circumstances when the ionization level is lower the signal change may only be a few per cent. A characteristic of the shorted signal appearing on practically all traces is its jagged appearance.

3) The wave that is re-reflected from the contact surface becomes a prominent part of the signal. At 1 mm. (Fig. 4b) it appears about 230 microseconds after the first reflection and at 100 microns it has reduced the end wall testing time to 30 microseconds.

The signal from the side wall also shows the gradual initial rise. All forms of the shorting effect are illustrated after the reflected wave passes over the film. It is evident from figure 14

that the first event after passage of the initial shock at a given station on the side wall will be either the passage of the contact surface or of the reflected wave, depending on the station and proximity of the contact surface to shock wave. At gauge No. 3 the reflected wave is seen at high pressures but at low pressures the contact surface passes first. This is indicated by the evident cooling in figure 4c not observed at higher pressures. On gauges No. 1 and No. 2 (Fig. 5a) the contact surface passes first even at higher pressures. Note how the time between the shock and onset of cooling decreases with decreasing pressure until at 10 microns the contact front quenches the flow before the initial rise has reached full theoretical value (Section I. 3. 4).

A further feature of the side wall signal not observed at the end wall is a gradual rise after the initial step even at 10 mm. (Fig. 5a). This is due to the fact that the glass backing of the film is not flush with the side wall, so the boundary layer flow does not develop parabolically. Since the primary purpose of the gauge was to record passage of the shock for triggering the timer, no attempt was made to correct this situation.

The times observed on the side wall between shock and contact front do not agree quantitatively with the theory developed by Roshko (Ref. 5) because the boundary layer effect is not the only mechanism determining the distance between shock wave and contact surface. In fact for pressures less than 10 mm. the most important factor is probably the slow formation of the shock wave (Fig. 6). At low pressures the testing time is several times larger than that predicted from measured Mach numbers by the boundary layer

considerations.

I.3.2 Average Mach number between films No. 2 and No. 3 vs. diaphragm pressure ratio. Figure 6. These results are compared with the predictions of simple perfect gas shock tube theory and show a very strong pressure dependence. At high pressures and low Mach numbers the Mach number M_{23} is very nearly the predicted value but the deviation from theory increases with increasing Mach number and decreasing pressure. The effect of diaphragm opening time on shock formation distance was discussed qualitatively by White in reference 4 and experimental results were presented showing that formation distance increased with increasing shock strength and increasing diaphragm pressure ratio. Thus the experimental results of reference 4 are consistent with figure 6.

However, in the present experiments the additional parameter p_1 was controlled so an additional piece of information may be obtained. Figure 6 illustrates that for a given p_1 the deviation from theory decreases with increasing Mach number i.e. with increasing p_4. This result is consistent with any ideas about the effect of diaphragm opening time on shock formation, since it is probable that the opening time decreases with larger force p_4 applied to the diaphragm. On the other hand, that this is not the only factor contributing to shock formation is indicated by the fact that for a given p_4 the deviation from theory decreases with increasing p_1.

The relatively large experimental scatter at low pressure indicates the further point that diaphragm opening time and therefore shock formation distance depend on other parameters than those

controlled in the experiment. These probably include variations in diaphragm scribing technique, etc.

I. 3. 3. Attenuation between two adjacent 10 inch intervals. Figure 7. The attenuation results show that the shock wave is accelerating at the end of the tube, a result consistent with the idea that the shock is not fully developed. The experimental scatter is very large for two reasons. The scatter indicated at the left hand end of each curve in figure 7 is 1 microsecond, the least count of the timer. However, the scatter observed at higher Mach numbers on each curve is 6 microseconds or more. It is expected that this is due to the variations in breakage of the diaphragm which influence the properties of a shock wave until the shock is fully developed and well away from the contact surface.

I. 3. 4. Heat transfer to wall gauges, Figure 8. These data are compared with the theory of heat transfer to side walls as developed by Rott and Hartunian (Ref. 11). A simple minded theory results from considering a wall placed in contact at time $t = 0$ with a compressible stationary gas at a different temperature. This is the theory covered by Roshko in reference 7 for heat transfer to end walls and involves the neglect of the displacement effect (Section II. 1). The result for the temperature jump at the wall surface is

$$\frac{\Delta T}{T_1} = \frac{c_{p_1}}{c_w} \sqrt{\frac{k\rho}{c_p} \Big/ \left(\frac{k\rho}{c}\right)_w} \left(\frac{h}{h_1} - 1\right) \qquad \text{(I. 1)}$$

where T is temperature, c specific heat, k thermal conductivity,

h specific enthalpy and ρ density. For a constant current gauge

$$\frac{\Delta E}{E} = \frac{\Delta R}{R} = \alpha_w \Delta T \qquad \text{(I. 2)}$$

where E is the voltage across a gauge, R its resistance and α_w the thermal coefficient of resistivity of the gauge material (platinum). Combining equations I. 1 and I. 2 and rewriting,

$$\frac{\Delta E}{E} = \sqrt{\frac{\beta_s}{\beta_w}} (\alpha_w T_1') \sqrt{\frac{p_1}{p_s}} \sqrt{\frac{\rho \mu}{\rho_1 \mu_1}} \left(\frac{h}{h_1} - 1 \right) \qquad \text{(I. 3)}$$

where $( )_s$ refers to the gas at S. T. P., $( )_w$ refers to properties of the wall, $( )_1$ refers to initial conditions, $\beta = \rho c_p k$, and μ is the viscosity.

The theory of Rott and Hartunian takes into account the motion of the gas past a side wall gauge by making a boundary layer analysis. The actual voltage jump $(\Delta E/E)'$ is given by

$$\left(\frac{\Delta E}{E}\right)' = K(M, Pr) \frac{\Delta E}{E} \qquad \text{(I. 4)}$$

where K is plotted in reference 10 and $\frac{\Delta E}{E}$ is given by equation I. 3.

In the experiment, traces of two consecutive wall gauges (No. 1 and No. 2, or No. 2 and No. 3) are recorded in each run. The initial jumps in voltage are averaged and are plotted against the average Mach number over that interval as obtained from the timer record. These are fitted to the theory at 10 mm. by choice of the

wall parameter $\alpha_w/\sqrt{\beta_w}$ which in this case is 0.076 c.g.s. As can be seen in figures 4 and 5 the height of the initial step at high pressures is well defined despite the subsequent gradual rise on the side wall gauges due to their protrusion into the flow. However, at p_1 = 0.1 mm. (Figs. 4c, 5c), the "knee" at the top of the initial rise has become so pronounced as to prevent a definite determination of $\Delta E/E$. The values plotted are taken at the base of the knee and therefore may be too low. On the other hand, the points for p_1 = 0.01 mm. represent the maximum signal attained in the initial rise (e.g. Fig. 5d).

It is evident that at the lowest pressure the gradual initial rise and early quenching combine to prevent the wall temperature from reaching the theoretical value. That this effect depends on the variations of diaphragm breakage is shown by the large scatter.

I.3.5. Heat transfer to end gauge. Figure 9. The initial jump in end gauge (No. 4) voltage is plotted against the average Mach number between gauges No. 2 and No. 3. A best fit between theory and experiment at high pressures is obtained by taking $\alpha_w/\sqrt{\beta_w}$ = 0.10 c.g.s. This value for platinum on Scotch splicing tape is very close to the value for platinum on glass.

The same difficulty in obtaining data at p_1 = 0.1 mm. is encountered here as in section I.3.4. The points indicated represent minimum values.

APPENDIX II

THE EQUATIONS FOR DIFFUSION IN AN IONIZED GAS

II. 1 Introduction

In this appendix a detailed derivation of the equations for diffusion in a partially ionized gas is presented. The purpose is two-fold: a) to exhibit the approximations implied by the final equations and, b) to illustrate the relation between any general problem of diffusion in an ionized gas and the simplified one considered in detail here. The complete set of equations describing a non-reacting ("frozen") three component gas (ions, electrons and neutral atoms) acted upon by electromagnetic body forces would consist of conservation equations for mass, momentum, energy and each species (Ref. 2, p. 698), equations for the flux of each species, of heat and of momentum as functions of the gradients of state and velocity (Ref. 2, p. 517 f.f.), equations for the body forces (Maxwell's equations, Ref. 12, pp. 18, 19), and equations of state.

The usual technique for simplifying this system is to abstract diffusion from the other processes covered by the equations, such as dissipation by viscosity and heat conduction, and convection of momentum and energy. The relevant equations become the various continuity equations and the relations between flux of species and gradients of state. In the present work, a slightly more general technique will be used.

The distinctive features of the problem considered here will be the electric body forces and the diffusion of the various

components. The body forces will appear in all the equations since they can effect a transport of mass, momentum or energy. They appear in the continuity equations (diffusion equations) as a "restoring" force to impede diffusion, can cause a non-zero pressure gradient across a boundary layer due to momentum transport, and can effect a transfer of energy in the absence of temperature gradients. Similarly, diffusion down a concentration gradient can transport internal or translational energy in the absence of thermal gradients.

It is desired to derive a set of equations which describes the one-dimensional model outlined in section 3.2: At time $t^* = 0$ a body of gas ($x^* > 0$) adjacent to a wall ($x^* < 0$) of known properties is instantaneously heated and ionized to constant uniform temperature T_∞, pressure p_∞ and ion number density n_∞. As discussed in section III.3, the temperature of the wall plays an important role in the boundary conditions. It is therefore natural in this problem to retain heat transfer for completeness. This aspect of the problem is precisely that worked out by Roshko for heat transfer to the end wall of a shock tube (Ref. 7) and the same scheme of approximation can be used: To first order the velocity of the mixture is assumed everywhere zero (higher orders can be computed by iteration on the full equations). It is immediately seen that for a compressible gas, where in general $\partial\rho/\partial t \neq 0$, the continuity equation is violated. From the analog offered by boundary layer theory it can be stated that the "displacement effect", i.e. the velocity that must be induced due to changes in density, is neglected. The equations are written down under this assumption and are then non-dimensionalized and

discussed in terms of two characteristic parameters, α the degree of ionization, and D the square root of the ratio of electron mass to atom mass. For small α the equations are further simplified and discussed.

The problem as stated is initially one dimensional and will remain so if body forces act only in the x direction. The restrictions implied by the one dimensionality are first discussed and then the equations are written down.

II.1.1 Maxwell's equations. The electromagnetic body force per unit volume in a fluid is (c.f. eq. II.9a)

$$\vec{f} = \omega\vec{E} + \vec{j} \times \vec{B} \qquad \text{(II.1)}$$

where ω is the volume charge density ($\omega = e(n_i - n_e)$, and $\vec{E}$, $\vec{j}$ and $\vec{B}$ are the electric field, current and magnetic field respectively, all in MKSQ units. For the class of problems in which there is a finite component of $\vec{j}$ in the $\vec{E}$- direction (taken to be the x-axis), the body force introduces a two-dimensionality unless $\vec{B} = 0$. Thus, Lorentz forces $(\vec{j} \times \vec{B})$ are not considered here. This situation arises without assumption in the particular problem of interest as follows: Initially $\vec{E} = \vec{B} = 0$. The wall at first induces a current and an electric field in the x-direction only. Thus curl $\vec{E} = 0$ initially and, from Maxwell's induction equation,

$$\frac{\partial \vec{B}}{\partial t} = - \text{curl } \vec{E} = 0 \qquad \text{(II.2)}$$

The magnetic field remains zero and $\vec{f} = \omega \vec{E}$ so that the problem remains one dimensional for all time.

The general expression for the current in an ionized gas is

$$\vec{j} = e(\vec{F}_i - \vec{F}_e) \tag{II.3}$$

where $\vec{F}$ is the flux across unit area in unit time. The electric field is not the only mechanism by which a difference in fluxes may be induced (we are interested here, for example, in diffusion) so the simple Ohm's law $\vec{j} = \sigma \vec{E}$ is not expected to apply generally in an ionized gas.

Of the remaining Maxwell equations, the ones that are not satisfied identically for one dimension are

$$\frac{\partial D}{\partial x} = \omega = e(n_i - n_e) \tag{II.4}$$

$$D = \varepsilon_o E \tag{II.5}$$

$$\frac{\partial D}{\partial t} + j = 0 \tag{II.6}$$

where D is the electric displacement, ε_o is the permeability of free space and where quantities without arrows from now on signify x-component. Equation II.6 is redundant since equations II.3, II.4 and the continuity equations II.8 lead to the same result.

II.1.2 Conservation equations. For generality the equations with zero total velocity are first written for any number of components and any body force X_j acting on a particle of the j^{th} species. They can be specialized to electromagnetic body forces by substitution

$$\begin{aligned} X_i &= e(E + v_i \times B) \\ X_e &= -e(E + v_e \times B) \\ X_n &= 0 \end{aligned} \tag{II.7}$$

As stated above, the total continuity equation is violated. The conservation of each species for a non-reacting mixture is expressed by

$$\frac{\partial n_j}{\partial t} + \frac{\partial F_j}{\partial x} = 0 \quad \text{(one-dimension)} \tag{II.8}$$

The momentum equation in the x direction is

$$\frac{\partial p}{\partial x} = \sum_{j=1}^{\nu} n_j X_j \tag{II.9}$$

Using equations II.7 and II.3, the right hand side becomes the well-known electromagnetic body force

$$\sum n_j X_j = \omega E + j \times B \tag{II.9a}$$

Thus, in this problem, though the "boundary layer" assumption is made, the pressure gradient does not vanish.

The energy equation written for one dimension is

$$\rho \frac{\partial \mathcal{E}}{\partial t} = - \frac{\partial Q}{\partial x} + \sum_{j=1}^{\nu} F_j X_j \tag{II.10}$$

where $\mathcal{E}$ is the energy per unit mass, Q the heat flow per unit area and time, and $F_j X_j$ is the transport of energy by the j^{th} species in the x direction. This latter term is a "dissipation" of energy and, for electromagnetic forces becomes the familiar joule heat

$$\sum F_j X_j = j E \tag{II.10a}$$

For B = 0 this becomes (c.f. eq. II.6)

$$\sum F_j X_j = - \frac{\partial}{\partial t} \frac{\mathcal{E}_o E^2}{2}$$

the rate of change of the energy stored in the electric field ($\mathcal{E}_o$, the permeability, not to be confused with $\mathcal{E}$, the energy).

II.1.3 Equations for mass and heat flux. Usually, to obtain the equations of mass flux, the flux F_j of the j^{th} species is defined as an integral over the distribution of molecular velocities, f_j,

$$F_j = n_j v_j = \int f_j v_j \, dv_j$$

where f_j is subsequently determined as an approximate solution to the Boltzmann equation. A similar technique is used to derive the heat flux equation. This method results in equations in which the diffusion coefficients and heat conductivity are expressed in terms of integrals over the potential functions of the particles. The applicability of the results is restricted by the specific assumptions which are made in working with the Boltzmann equation; for example the assumption of binary encounters required for its derivation (requiring a further discussion in the case of an ionized gas in which "long range" forces are present) and the expansion procedures necessary for obtaining a solution to the equation.

The same equations can be derived by the more general techniques of irreversible thermodynamics (Ref. 2, p. 704 f.f.) with fewer restrictive assumptions, indicating that they are much

more general than would be expected from the above derivation. The assumptions are simply that all species have the same temperature T and that the various fluxes can be expressed as linear combinations of the various gradients of state. These assumptions are typical for the Navier-Stokes equations and are usually interpreted as implying "small" departures from equilibrium.

The assumption of equal temperature implies that the body forces do not give energy preferentially to one particular species. This means that the kinetic energy gained from the field by the electrons must be smaller than thermal energy. For an electric field, the energy gained by an electron in one mean free path must be smaller than the thermal energy, $e E \Lambda_\infty / kT < 1$. The coefficients in the linear relations between the fluxes and gradients of state (diffusion coefficients and heat conductivity) remain undetermined and must be obtained from experiment or, in special simple cases, by resort to kinetic theory.

The result for a one-dimensional monatomic gas in which the coefficient of thermal diffusion is much smaller that the usual binary diffusion coefficient D_{jk} ($D_{jk} = D_{kj}$) is (Ref. 6, p. 517 and 522, using eq. I. 9)

$$\sum_{\substack{k=1 \\ k\neq j}}^{\nu} \frac{n_j F_k - n_k F_j}{\rho^2 D_{jk}} = d_j \,, \qquad \sum_{j=1}^{\nu} m_j F_j = 0 \tag{II.11}$$

$$d_j = \frac{\partial}{\partial x}\frac{n_j}{\rho} + \frac{n_j}{p}\left(\frac{1}{\rho}\frac{\partial p}{\partial x} - X_j\right) \,, \qquad \sum_{j=1}^{\nu} d_j = 0 \tag{II.12}$$

$$Q = -K \frac{\partial T}{\partial x} + \frac{5}{2} kT \sum_{j=1}^{\nu} F_j \qquad \text{(II. 13)}$$

where

$$\eta = \sum_{j=1}^{\nu} n_j$$

$$\rho = \sum n_j m_j$$

ν = number of components

X_j = body force acting on j^{th} component

Q = heat flux

K = heat conductivity for the mixture

Writing out equation (II. 11), for the fluxes of electrons and ions in a three-component gas (third component neutral particles) gives

$$F_i = -D_{in}\,\eta\, d_i \frac{1 - \frac{n_i}{\eta}\left[1 - \frac{D_{en}}{D_{ei}}\right] - \frac{n_e}{\eta}\left[1 - \frac{m_e}{m_n}\right] + \frac{n_i}{\eta}\frac{d_e}{d_i}\left[\frac{D_{en}}{D_{ei}} - \frac{m_e}{m_n}\frac{D_{en}}{D_{in}}\right]}{1 - \frac{n_i}{\eta}\left[1 - \frac{m_i D_{en}}{m_n D_{ei}}\right] - \frac{n_e}{\eta}\left[1 - \frac{m_e}{m_n}\frac{D_{in}}{D_{ei}}\right]} \qquad \text{(II. 11a)}$$

$$F_e = -D_{en}\,\eta\, d_e \frac{1 - \frac{n_e}{\eta}\left[1 - \frac{D_{in}}{D_{ei}}\right] - \frac{n_i}{\eta}\left[1 - \frac{m_i}{m_n}\right] + \frac{n_e}{\eta}\frac{d_i}{d_e}\left[\frac{D_{in}}{D_{ei}} - \frac{m_i}{m_n}\frac{D_{in}}{D_{en}}\right]}{1 - \frac{n_e}{\eta}\left[1 - \frac{m_e}{m_n}\frac{D_{in}}{D_{ei}}\right] - \frac{n_i}{\eta}\left[1 - \frac{m_i}{m_n}\frac{D_{en}}{D_{ei}}\right]} \qquad \text{(II. 11b)}$$

It is immediately seen that these equations can be greatly simplified if it is possible to assume n_i/η and n_e/η so small that the complicated fractions on the right hand sides of both

equations are essentially 1. This is the case for slightly ionized gases (n_e, $n_i \doteq 0$) and equations II. 11 become

$$F_i \doteq - D_{in} \eta \, d_i$$

$$F_e \doteq - D_{en} \eta \, d_e \qquad \text{(II. 11c)}$$

II. 1. 4. Equations of state. It is assumed that each species is thermally and calorically perfect. Summing up the individual equations of states gives

$$p = \eta k T \qquad \text{(II. 14)}$$

The energy per unit mass $\mathcal{E}$ appearing in equation II. 9 is the weighted sum of the individual energies, $\mathcal{E}_j = \frac{3}{2} \frac{kT}{m_j}$

$$\mathcal{E} = \frac{1}{\rho} \sum n_j m_j \mathcal{E}_j = \frac{3}{2} \frac{\eta k T}{\rho} = \frac{3}{2} \frac{p}{\rho} \qquad \text{(II. 15)}$$

II. 2 Parametrization and Non--dimensionalization.

To examine the details of the approximation II. 11c the complete set of equations is now written in terms of two characteristic parameters, the ratio of electron mass to atom mass and the degree of ionization. It is evident that these parameters will appear explicitly in the equations and implicitly in D_{jk} and K. Kinetic theory is used to make the latter dependence explicit as follows:

a) It is assumed that

$$D_{jk} = \sqrt{\frac{m_j + m_k}{m_j m_k}} \times f \qquad \text{(II. 16)}$$

where the function f is the same for all j and k (i.e. electrons diffuse through ions in the same way as they diffuse through neutrals, etc.). This permits the expression of the ratios of diffusion coefficients appearing in equations II. 10a and II. 10b in terms of the single parameter $D = \sqrt{\frac{m_e}{m_n}}$ (= .0037 for argon atoms);

$$\frac{D_{in}}{D_{en}} = \sqrt{2}\, D \left(1 - \frac{1}{4} D^2 + \ldots\right)$$

$$\frac{D_{in}}{D_{ei}} = \sqrt{2}\, D \left(1 - \frac{1}{4} D^2 + \ldots\right) \qquad \text{(II. 17)}$$

$$\frac{D_{en}}{D_{ei}} = 1 - \frac{1}{2} D^4 + \ldots$$

b) The thermal conductivity K of a mixture of gases can be written to first order in α, the degree of ionization ($= \frac{n_\infty}{\eta_\infty}$ where n_∞ is the number of electrons per volume at $x = \infty$), and D by using a rather complicated relation derived from kinetic theory (Ref. 2, p. 535, eq. 8.2-36). The thermal conductivity of a pure electron gas K_e is used as a reference but can be transformed to the more familiar conductivity for pure atoms K_n by a relation analogous to II. 16 $K_n \doteq D\, K_e (1 + \ldots)$. The result is

$$K \doteq K_e \left(D + \frac{2}{3} \frac{\alpha n}{\eta}\right) \qquad \text{(II.18)}$$

The non-dimensionalization is carried out using quantities at $x = \infty$ where conditions are uniform and equal to the initial conditions ($n_{i\,\infty} = n_{e\,\infty} \equiv n_\infty$ and $E_\infty = 0$) and for the case in which the body force is due to the electric field (eq. II. 7 with $B = 0$),

$$x^* = \frac{x}{\lambda_\infty} \quad \text{where} \quad \lambda_\infty = \left(\frac{\varepsilon_o k T_\infty}{e^2 n_\infty}\right)^{\frac{1}{2}} \text{, the Debye length}$$

$$t^* = \frac{t}{\tau} \quad \text{where} \quad \tau = \frac{\lambda_\infty^{\,2}}{(D_{en})_\infty}$$

$$N = \frac{n_i}{n_\infty} \quad , \quad n = \frac{n_e}{n_\infty} \quad , \quad \eta^* = \frac{\eta}{\eta_\infty} \qquad \text{(II.19)}$$

$$T^* = \frac{T}{T_\infty} \quad , \quad p^* = \frac{p}{p_\infty}$$

$$\alpha = \frac{n_\infty}{\eta_\infty} \quad , \quad D = \sqrt{\frac{m_e}{m_n}}$$

$$F_i^* = \frac{F_i \lambda_\infty}{(D_{en})_\infty n_\infty} \quad , \quad E^* = \frac{e E \lambda_\infty}{k T_\infty} \quad , \quad Q^* = \frac{Q \lambda_\infty}{(K_e)_\infty T_\infty}$$

The full set of equations with each term to lowest order in α or D are written below. In rewriting the equations for energy a non-dimensional number analogous to the Lewis number appears and can be evaluated approximately

from simple kinetic theory;

$$Le' = \frac{k\ \eta_\infty\ (D_{en})_\infty}{(K_e)_\infty} \doteq \frac{1}{3} \qquad \text{(II. 20)}$$

Diffusion of Ions

$$F_i^* \doteq - d_i^*\ D\ \frac{1 - N\alpha\left[\frac{D^4}{2} - \frac{d_e^*}{d_i^*}\left(1 - \frac{D}{\sqrt{2}}\right)\right] - n\alpha\left(1 - D^2\right)}{1 - N\alpha D^2 - n\alpha\left(1 - \sqrt{2}\, D^3\right)}$$

$$d_i^* = \gamma^*\ \frac{D_{en}}{(D_{en})_\infty}\left[\frac{\partial}{\partial x^*}\ \frac{N}{\gamma^*} + \frac{N}{p^*}\left(\frac{1}{\gamma^*}\ \frac{\partial p^*}{\partial x^*} - E^*\right)\right] \qquad \text{(II. 21)}$$

$$\frac{\partial F_i^*}{\partial x^*} = - \frac{\partial N}{\partial t^*}$$

Diffusion of Electrons

$$F_e^* \doteq - d_e^*\ \frac{1 - n\alpha\left[1 - \sqrt{2}\, D - \frac{d_i^*}{d_e^*}\ \frac{3}{2\sqrt{2}}\ D^3\right] - N\alpha D^2}{1 - N\alpha D^2 - n\alpha\left(1 - \sqrt{2}\, D^3\right)}$$

$$d_e^* = \gamma^*\ \frac{D_{en}}{(D_{en})_\infty}\left[\frac{\partial}{\partial x^*}\ \frac{n}{\gamma^*} + \frac{n}{p^*}\left(\frac{1}{\gamma^*}\ \frac{\partial p^*}{\partial x^*} + E^*\right)\right] \qquad \text{(II. 22)}$$

$$\frac{\partial F_e^*}{\partial x^*} = - \frac{\partial n}{\partial t^*}$$

Momentum Equation

$$\frac{\partial p^*}{\partial x^*} = E^* (N - n) \qquad \text{(II. 23)}$$

Diffusion of Energy

$$Q^* \doteq - \frac{K_n}{(K_n)_\infty} \left(D + \frac{2\alpha n}{3\eta^*} \right) \frac{\partial T^*}{\partial x^*} + \frac{5}{2} Le' \alpha T^* \left(D^2 F_i^* + (1 - D^2) F_e^* \right)$$

(II. 24)

$$\frac{\partial Q^*}{\partial x^*} = Le' \left[- \frac{3}{2} \eta^* \frac{\partial T^*}{\partial t^*} + \frac{3}{2} p^* \frac{\partial}{\partial t^*} \ln \left(1 - \alpha n + \alpha D^2 (n + N) \right) - \alpha \frac{\partial}{\partial t^*} \frac{E^{*2}}{2} \right]$$

Maxwell's Equation

$$\frac{\partial E^*}{\partial x^*} = N - n \qquad \text{(II. 25)}$$

Equation of State

$$p^* = \eta^* T^* \qquad \text{(II. 26)}$$

Note that the equation for the flux of the j^{th} species contains the generalized gradient d_k^* of the k^{th} species.

II. 2. 1. Relation between fluxes and field. Combining the continuity equations for electrons and ions with the electro-

static equation (II.25) and integrating over x^* using the condition of uniformity at $x^* = \infty$ results in the useful relation

$$\frac{\partial E^*}{\partial t^*} = F_e^* - F_i^* \qquad \text{(II. 27)}$$

II. 2. 2. Slightly ionized gas. The approximation of equation II. 11c can now be made for the complete set of equations by setting $\alpha = 0$. From equation II. 23, the pressure becomes constant ($p^* = 1$). The equations become (taking $Le' = 1/3$)

$$\frac{\partial N}{\partial t^*} = D \frac{\partial}{\partial x^*}\left[\eta^* \frac{D_{en}}{(D_{en})_\infty}\left(\frac{\partial}{\partial x^*}\frac{N}{\eta^*} - N E^*\right)\right]$$

$$\frac{\partial n}{\partial t^*} = \frac{\partial}{\partial x^*}\left[\eta^* \frac{D_{en}}{(D_{en})_\infty}\left(\frac{\partial}{\partial x^*}\frac{n}{\eta^*} + n E^*\right)\right]$$

$$\frac{\partial T^*}{\partial t^*} = \frac{2D}{\eta^*}\frac{\partial}{\partial x^*}\left[\frac{H_n}{(H_n)_\infty}\frac{\partial T^*}{\partial x^*}\right] \qquad \text{(II. 28)}$$

$$\frac{\partial E^*}{\partial x^*} = N - n \quad , \qquad \eta^* T^* = 1$$

The ternary diffusion process (in which the flux of electrons, say, depends on the gradient of ions) has been reduced to two binary diffusion processes which are coupled by the body force and effects of heat transfer. T^* (and therefore η^*) is determined by the standard heat transfer problem with appropriate thermal boundary conditions which can be solved using the Howarth Transformation. To fix ideas the heat transfer can be eliminated by considering a simple subcase in which

$T^* = \text{const.} = 1$. Then $\eta^* = 1$ and $\frac{D_{en}}{(D_{en})_\infty} = 1$, and we obtain

$$N_{t^*} = D\,(N_{x^*x^*} - (NE^*)_{x^*})$$

$$n_{t^*} = n_{x^*x^*} + (nE^*)_{x^*} \qquad \text{(II. 29)}$$

$$E^*_{x^*} = N - n$$

where subscripts $(\ )_t$ and $(\ )_x$ now signify partial differentiation. Initial conditions:

$$n\,(x^*,\ 0) = N\,(x^*,\ 0) = 1\ ,\quad E^*\,(x^*,\ 0) = 0$$

These equations are discussed in detail in appendix IV.

II. 3 Isothermal Equilibrium

A very important subcase of II. 29 for the shock tube experiments is the steady state case ($\frac{\partial}{\partial t^*} = 0$, isothermal equilibrium). The two diffusion equations can be integrated once with respect to x^* using the conditions at $x^* = \infty$,

$$\frac{N_{x^*}}{N} = E^*\ ,\quad \frac{n_{x^*}}{n} = -E^*$$

Using the definition of a potential V^*,

$$V^*_{x^*} \equiv -E^* \qquad \text{(II. 30)}$$

the equations can be integrated again

$$N(x^*) = e^{-V^*(x^*)}$$

$$n(x^*) = e^{V^*(x^*)} \qquad \text{(II.31)}$$

$$V^*_\infty \equiv 0$$

Equation II.31 is the familiar Boltzmann distribution for equilibrium. Combining with the third equation II.29 gives,

$$V^*_{x^*x^*} = \sinh V^* \qquad \text{(II.32)}$$

Boundary conditions:

$$V^*(\infty) = V^*_{x^*}(\infty) = 0, \quad V^*(0) = V^*_o$$

The solution to this equation is (Refs. 8 and 13)

$$2x^* = \ln \frac{\tanh \frac{V^*_o}{4}}{\tanh \frac{V^*}{4}} \quad ; \quad V^* = 4 \tanh^{-1} \left(e^{-2x} \tanh \frac{V^*_o}{4}\right) \qquad \text{II.33)}$$

Note that for $n(0) \gtrless 1$ ("hot wall" or "cold wall", as defined in section III.3), then $N(0) \lesseqgtr 1$ and $V^*_o \gtrless 0$. The curves for n and N for these two cases are plotted in figure 15. Note that for any boundary condition $n(0)$, the x^*-axis is shifted so that the y-intercept on the appropriate curve is $n(0)$.

It can be seen that the departure from neutral distribution is large only for $x^* < 1$. This is the well-known result that the decay distance for the effect of a wall in equilibrium is the Debye Length.

II. 4 Ambipolar Diffusion

A customary approximation which will be referred to in appendix IV is known as ambipolar diffusion. From the steady state results it is argued that charge separation tends to be slight except near a wall, so that in some region it is possible to assume $n \doteq N$. This over-determines the equations II. 29. The two diffusion equations give

$$E^* = \frac{1 - D}{1 + D} \frac{n_{x^*}}{n}$$

$$n_t^* = \frac{2D}{1 + D} n_{x^*x^*} \qquad \text{(II. 34)}$$

and the electrostatic equation serves as a check for the range of validity of the assumption. If, as is customarily done, the boundary condition is taken as $n(0) = N(0) = 0$, then

$$N(x^*, t^*) = n(x^*, t^*) = \operatorname{erf} \frac{x^*}{2\sqrt{\frac{2D}{1+D} t^*}}$$

$$E^* = -\frac{1-D}{\sqrt{2\pi D(1+D)\, t^*}} \frac{e^{-\frac{x^{*2}}{8D} t^*}}{\operatorname{erf} \frac{x^*}{2\sqrt{\frac{2D}{1+D} t^*}}} \qquad \text{(II. 35)}$$

The electrostatic equation states that the approximation is valid for $E_{x^*} << 1$ which is satisfied if

$$\frac{x^*}{2\sqrt{\frac{2D}{1+D}t^*}} \doteq \frac{x^*}{2\sqrt{2Dt^*}} \gg 1$$

A further condition for validity deduced from the solution at large distances (Sec. IV.2) is that $\frac{x^*}{2\sqrt{t^*}} \ll 1$.

In the region $\frac{x^*}{2\sqrt{\frac{2D}{1+D}}\,t^*} \ll 1$ the field is given by

$$E^* \doteq -\frac{1-D}{1+D}\,\frac{\sqrt{\pi}}{2x^*} \qquad \text{(II.36)}$$

The infinity at $x^* = 0$ is a direct consequence of the boundary condition $n(0) = N(0) = 0$ and is discussed in section IV.2.

The fluxes are given by

$$F^* = -\frac{2D}{1+D}\,n_{x^*} = -\sqrt{\frac{\frac{2D}{1+D}}{\pi t^*}}\; e^{-\frac{x^{*2}}{\frac{8D}{1+D}t^*}}$$

In particular

$$F^*(x^*=0) = -\frac{1}{\sqrt{\pi}}\sqrt{\frac{2D/1+D}{t^*}} \qquad \text{(II.37)}$$

APPENDIX III

THE ROLE OF THE WALL

III. 1 Introduction

As outlined in section 3. 2, the purpose of the theoretical investigation is to describe the details of a one-dimensional charge diffusion process represented by the following model: At time $t = 0$ a body of gas $(x > 0)$ adjacent to a wall $(x < 0)$ of known properties is instantaneously heated and ionized to uniform temperature T_∞, pressure p_∞ and ion number density n_∞. No net charge is drawn from the gas by external fields (zero current in the wall). The presence of the wall affects the charge distribution as discussed below and a redistribution of charge in the gas takes place by diffusion. Evidently the equations for the response of the gas, the initial conditions $(t = 0)$ and the boundary conditions at $x = \infty$ (identical to the initial conditions) can be written down from a consideration of the physics of the partially ionized gas alone (Appendix II). However, the conditions at $x = 0$ are dependent upon the properties of the wall. In general, the solution to the problem for $x > 0$ requires the solution of a similar problem for $x < 0$ with suitable matching of the solutions at $x = 0$. Thus the "boundary conditions" at $x = 0$ are not prescribed a priori but are actually matching conditions between two solutions. Because of the complexity of a complete description (in general requiring quantum mechanical computations) an inquiry is made to determine under what circumstances approximate matching conditions can be written

in the form of a priori boundary conditions. Von Laue, Schottky and others (as summarized by Fowler (Ref. 8)) have effected an approximate matching of the thermodynamics of the two regions for the case of a plasma in isothermal equilibrium with a metallic container. This results in an explicit condition on electron density at $x = 0$ (cf. below). Langmuir (Ref. 13) has patched together several subregions in a more detailed analysis of a neutral two component equilibrium plasma. The (statistical) equilibrium discussed here is the same as that encountered in any problem where pressure forces balance other non-dissipative forces (inertial, gravitational or electrostatic) in an isothermal enclosure (e.g. an isothermal atmosphere). The temperature is uniform throughout but not necessarily other properties such as density and entropy.

For the time dependent (non-equilibrium) two component plasma we follow Fowler's point of view. As seen in appendix IV, thermodynamic equilibrium for the electrons is a very important limiting case. This is not surprising since the equations for the gas mixture as written are valid for small fields, i.e. small departures from equilibrium. However, the non-equilibrium behavior of the ions distinguishes this problem from those above, and will be discussed in detail.

From the discussion below, it is apparent that the properties of a conducting wall (e.g. very narrow induced charge sheets) lend themselves to representation as explicit boundary conditions at $x = 0$. Thus for simplicity the discussion will be restricted to the particular case of a metallic wall.

The thermodynamic system representing this problem (Fig. 3) is divided into two bulk phases (which will be called the "metal phase" and the "gas phase") separated by a third phase, the "surface phase". The gas phase represents the region occupied by the partially ionized gas ($x > 0$), the metal phase ($x < 0$) is the wall which bounds the gas phase and the region in which the properties of the system undergo a continuous transition from metal to gas phase is the surface phase.

In this appendix the properties of the metal and surface phases will be discussed in detail with the idea of fixing boundary conditions for use in the analysis of the gas phase.

III. 2 The Metal Phase

It is sufficient here to use the elementary free electron theory of metals in which the metal consists of a crystalline structure with an average of one electron per atom perfectly free to move about. The ions are fixed and their positive charge is assumed constant and uniform (i.e. the crystal is structureless). The electrons are treated quantum mechanically as an ensemble of free particles with half integral spin, therefore subject to the condition that the wave function of the ensemble be antisymmetric with respect to interchange of space and spin coordinates of any two electrons (Pauli Exclusion Principle). This results in Fermi Dirac Statistics. From these statistics the thermodynamic properties of the metal may be derived. For example the chemical potential μ of the electrons is computed to be

(Ref. 8)

$$\mu \doteq -e\phi \qquad \text{(III. 1)}$$

where ϕ is the work function of the metal in volts. This is different than the chemical potential for electrons comprising a classical perfect gas ($e^2/4\pi\,\varepsilon_o\, n_e^{-\frac{1}{3}} \ll k\,T$ in formula III. 3 below),

$$\mu = k\,T \ln \frac{n_e h^3}{2(2\pi\, m_e k\, T)^{3/2}} \qquad \text{(III. 2)}$$

We now make some qualitative arguments to deduce some of the well-known properties of metals, establishing a point of view useful for the subsequent discussion of boundary conditions.

III. 2. 1. Electronic emission. The difference in statistics between the metal phase and gas phase creates a situation very analogous to evaporation in a system of two phases in contact (condensed and vapor). The most important characteristic of the electron ensemble in a metal is its high number density, $n_m \sim 10^{29}\ M^{-3}$. Real gas effects (e.g. condensation) can be expected in any charged gas when conditions are such that the inter-particle (coulomb) potential energy is larger than or equal to the thermal energy,

$$\frac{e^2}{4\pi\,\varepsilon_o (n_{r.g.})^{-1/3}} \sim k\,T \;; \qquad n_{r.g.} \sim \left(\frac{4\pi\,\varepsilon_o\, kT}{e^2}\right)^3 \qquad \text{(III. 3)}$$

At room temperature $n_{r.g.} \sim 10^{22}\ M^{-3} \ll n_m$. Thus the electrons in the metal are, classically speaking, a condensed phase. (On the other hand, a typical electron density in the gas phase is $n_\infty \sim 10^{15}\ M^{-3}$ (c.f. Table I) therefore constituting a classical perfect gas.)

For small fields ($E(0) < 10^8$ V/M) the "evaporation" from this condensed phase is thermionic emission. Relations describing it may be derived by considering the condensed and vapor phases (the metal and electron atmosphere) in isothermal equilibrium at a temperature $T = T_\infty$. However, there are other components in the system which may not be in equilibrium, such as the metal ions which are assumed fixed and therefore not evaporating. Such a partial equilibrium for two bulk phases in contact is known as contact equilibrium (Ref. 14, p. 338). It is treated by requiring the free enthalpy (chemical potential) of each component that is in equilibrium to be the same in both phases. For the electron atmosphere, where in general the density and therefore the free enthalpy varies within the gas phase (Eq. III. 2) the free enthalpy must be continuous at the interface (matching condition for equilibrium). Equating equations III. 1 and III. 2 at the interface gives

$$n_e(0) = \frac{2(2\pi m_e k T_\infty)^{1/2}}{h^3}\, e^{-\frac{e\phi}{kT_\infty}} \qquad \text{(equilibrium)} \qquad \text{(III. 4)}$$

Setting $e\phi/k T_\infty \equiv \phi^*$ and $a_o = 4\pi \epsilon_o h^2/m_e e^2 = 5 \times 10^{-11}$M. (the first Bohr radius) and using further definitions from equations II. 19 results in

$$n(0) = 4\sqrt{2 n_\infty \lambda_\infty^3 \left(\frac{\lambda_\infty}{a_o}\right)^3}\; e^{-\phi^*} \qquad \text{(equilibrium)} \qquad \text{III. 4a)}$$

This is the explicit boundary condition mentioned in section III. 1 for the case of steady state thermodynamic equilibrium. The density of the electrons at the wall is a function only of the temperature and the work function of the wall material.

The thermionic current, defined as the current which would be measured if the electrons emitted by the wall were drawn to a collector by an electric field, can be computed from equilibrium considerations so long as it can be assumed that the flux <u>from</u> the wall is the same with or without the equilibrium electron atmosphere. For equilibrium the flux <u>from</u> the wall is equal to the flux <u>to</u> the wall. The flux to the wall from the atmosphere can be computed from the simple free path theory for diffusion: The flux per unit area from the right across any plane, say $x = 0$ in figure 3, is equal to $n_e(x = \Lambda)\ \bar{c}_e/4$ where the density n_e is evaluated one electron mean free path (Λ) away from the plane. If the plane $x = 0$ is situated in a bulk phase there is also a flux from the <u>left</u> equal to $n_e(x = -\Lambda)\ \bar{c}_e/4$. The net flux to the right is

$$F_e(x = 0) = \frac{\bar{c}_e}{4}\left(n_e(x = -\Lambda) - n_e(x = \Lambda)\right) \qquad \text{(III. 5)}$$

The right hand side can be expanded in a Taylor series around $x = 0$ and, if $\Lambda \dfrac{\partial^2 n_e}{\partial x^2} \Big/ \dfrac{\partial n_e}{\partial x} \ll 1$, then

$$F_e\ (x = 0) = -\frac{\Lambda\, \bar{c}_e}{2} \left(\frac{\partial n_e}{\partial x}\right)_{x = 0} \qquad \text{(III. 5a)}$$

On the other hand, if the plane $x = 0$ is at the edge of a bulk phase as with the isothermal electron atmosphere, the flux from the gas will simply be given by

$$F_{eg}\ (x = 0) = -\frac{\bar{c}_e}{4}\ n_e\ (x = \Lambda) \qquad \text{(III. 6)}$$

Once again expanding around $x = 0$, this expression becomes, providing $\Lambda \dfrac{\partial n_e}{\partial x} \Big/ n_e \ll 1$,

$$F_{eg}\ (x = 0) = -\frac{\bar{c}_e}{4}\ n_e\ (x = 0) \qquad \text{(III. 6a)}$$

Note that for $n_e\ (x = 0) = 0$ expression III. 6 must be used. Non-dimensionalizing as above and taking $(D_{en})_\infty = \dfrac{\bar{c}_e\, \Lambda_\infty}{3}$ gives

$$F^*_{eg}\ (0) = -\frac{3}{4}\ \frac{\lambda_\infty}{\Lambda_\infty}\ n\ (0) \qquad \text{(equilibrium)} \qquad \text{(III. 6b)}$$

The flux from the wall (thermionic emission) is given by equations III. 6, 6a, 6b.

When the temperature of an emitter is very low and thermionic emission is correspondingly low, excitation of metal electrons by external energy sources and subsequent emission may be the rate determining process. For radiation impinging on the wall with energy larger than ϕ, the work function, the emission process is the photoelectric effect. If the flux of such photons to unit area of the surface is much larger than the thermionic current, photoelectric current will be important. This process is discussed in reference 8, p. 546 and reference 15. Another external source of energy is provided when particles collide with the surface. Particles with energies larger than the work function can be expected to cause electron emission.

The early investigators (e.g. Ref. 13) were interested in hot emitting cathodes so the "evaporation" formulas III. 4 were applicable. However, for a cold wall, it is expected that one of the latter processes might be important (sec. IV. 3).

III. 2. 2. Induced charge sheets. It is well known from Maxwell's equations that an electric field within a uniform conductor tends to a uniform value $E = j/\sigma$, any perturbations thereof decaying with a characteristic time $T = \varepsilon_o/\sigma$ (Ref. 12, p. 23). Thus, in electrostatics, $E = 0$ everywhere inside the conductor and, from equation II. 4 also $\omega = 0$. If there is a net charge in the conductor it must lie on the surface. The integral of equation II. 4 across the surface gives the jump in field from zero inside to $E(x = 0)$ just outside

$$\left[E\right] = E(0) = \frac{\omega_s}{\varepsilon_o} \qquad \text{(III. 7)}$$

where ω_s is the surface charge per unit area.

The actual (finite)thickness of the layer of charge near the surface can be estimated by evaluating the characteristic length of equation II.4 rewritten in terms of the potential V ($\partial V/\partial x \equiv - E$) where V is taken equal to the average energy of electrons within the metal ($\bar{V}_m \sim$ 5 volts). This defines a "Debye length" for a metal,

$$\lambda_m = \left(\frac{\varepsilon_o \bar{V}_m}{e\, n_m} \right)^{\frac{1}{2}} \qquad \text{(III.8)}$$

Taking $n_m \doteq 10^{29}$ leads to $\lambda_m \doteq 5 \times 10^{-11}$ M. Thus the thickness of the charge sheet and the time required to form this sheet under any given circumstances ($T \sim 10^{-19}$ sec.) are much shorter than any lengths and times characteristic of the processes in the gaseous phase (from Eqs. II.19 and Table I typically $\lambda_\infty \sim 10^{-5}$ M, $\tau \sim 10^{-9}$ S at room temperature).

A test of the consistency of this result is to determine from equation III.7 whether the removal, say, of all the electrons from the volume $1\ m^2 \times \lambda_m$ at $x = 0$, leaving the ions fixed with a net charge of $\omega_s = e n_m \lambda_m$, gives reasonable jumps in fields.

$$E(0) = \frac{e n_m \lambda_m}{\varepsilon_o} \doteq 10^{11}\ \text{V/M}$$

In the gas phase we expect the absolute value of the non-dimensional electric field (defined in eq. II.19) to be no larger than 10 at large time (c.f. eq. IV.6);

$$|E^*| = \frac{e|E|\lambda_\infty}{k T_\infty} \sim 10 \qquad \text{(III. 10)}$$

so that, taking room temperature and $\lambda_\infty \doteq 2 \times 10^{-5}$ M.,

$$|E\ (0)| \sim 10^4 \quad \text{V/M}$$

The fact that any electrostatic response of the metal will appear as a charge sheet on the surface (i.e. in the surface phase) suggests that for the purposes of the analysis of the gas phase it is sufficient to represent it as a delta function at $x = 0$. In other words the electrostatic behavior of the conductor can be represented as a condition at the boundary. It can be borne in mind that, for our application, the delta function actually represents a net volume charge concentration ω that is an extremely small perturbation on the total electron charge density (en_m); $\omega / en_m \sim 10^{-7}$. This fact supports the conclusion mentioned in section III. 2. 1 that reasonable fields have little effect on thermionic emission, the calculation of which assumes uniform electron density n_m within the metal.

In summary, the metal phase will be considered to consist of a uniform distribution of free electrons with the properties deduced above, and the thin charge sheets that are induced by external fields will be considered as part of the surface phase.

III. 3 The Surface Phase

The two most important features of the surface phase are charge sheets and recombination of electrons with gas ions. Recombination depends to a certain extent on the nature of the charge sheet. This point will be illustrated qualitatively in this section.

The sign of the charge sheet will depend on the relation between the initial conditions and the ultimate condition of equilibrium. For example, if the initial electron density (n_∞) is larger than the equilibrium density $n_e(0)$ then initially there will be a larger flux of electrons to the wall than from it. The surface will take on a negative charge ω_s equal and opposite to the integral over all x of the net positive charge remaining in the gas phase (conservation of charge). (The contribution of ion flux to the wall can, to a first approximation, be neglected (compare eqs. IV. 5) unless $n(0) \sim 1$ and $N(0) \ll 1$.) This situation can be called the "cold wall" ($n(0) < 1$ as given by eq. III. 4a). For the "hot wall" ($n(0) > 1$) the initial flux of electrons to the wall is less than from the wall. This leaves a net negative charge in the gas and a positive sheet of equal magnitude on the wall.

III. 3. 1. The cold wall. $n(0) < 1$ occurs in the shock tube experiments under consideration. If complete equilibrium were possible the charge distribution would satisfy equation II. 33 for $n(0) < 1$ (Fig. 15). In this case $V_o < 0$ and therefore $N(0) > 1$. However, in the actual case recombination takes place at the wall. The wall therefore acts as a sink of ions and it necessarily follows

that $N_i(0) < 1$, precluding ionic equilibrium. Recombination is, for the cold wall, decisively important.

The nature of the ion sink can be seen qualitatively from the properties of a metal wall outlined in section III. 2. 2. The surface phase is defined as the region containing the interface between gas and metal and is shown to contain a total net charge equal and opposite to the total net charge in the gas. If an ion enters the surface phase, the gas phase loses and the surface phase gains one plus charge. Once the ion is part of the surface phase, the relaxation time for attainment of the equilibrium appropriate to the new situation is $T \sim 10^{-19}$ seconds. The ion "changes its identity" within 10^{-19} seconds. For the cold wall (electron sheet) the ion becomes a loss of one electron from the sheet within this time, i.e. for all practical purposes it "recombines". Stated from another point of view, the probability that an electron will be at the point of impact of any ion colliding with the wall is unity (averaged over time intervals larger than T). It is impossible for there to be an accumulation of ions on the surface if there is an electron sheet. Not only does the metal wall comprise a massive third body for adsorbing the heat of recombination but it acts as an infinite source of electrons. The rate of recombination can be taken as the small but finite rate of loss of ions from the gas to the wall. To the extent that the free electron theory of metals applies to a wall material, a cold wall is perfectly catalytic to ion electron recombination.

III. 3. 2. The hot wall. This is the case originally studied (e.g. Ref. 13) with reference to the behavior of heated cathodes (esp. cesiated tungsten) in vacuum tubes. For equilibrium

$n(0) > 1$ and $N(0) < 1$. There is a net negative charge in the gas phase (due to large emission from the walls) and an equal positive sheet at $x = 0$. The sheet would be expected to consist of both a net excess of fixed metal ions and a number of gas ions that have become part of the surface phase (adsorbed). It is plausible that the paucity of electrons at $x = 0$ and the adsorbed ion sheet could affect recombination or at least negate its effect to the extent that there could be a finite flux of ions <u>from</u> the wall equal to the flux to the wall, thus achieving complete isothermal equilibrium

We are not interested in the details of this case but merely wish to point out how the same model could lead to fundamentally different results for the cold wall and hot wall.

APPENDIX IV

CHARGE DIFFUSION IN A SLIGHTLY IONIZED GAS

IV. 1 Introduction

For the purpose of describing the experiments in the shock tube, the results of the general definitions and discussion in appendices II and III are now applied to the case of a slightly ionized gas. The qualitative properties of the equations and boundary conditions for the gas phase are exhibited. They serve to define and clarify the approximations implied by some of the common ideas about the diffusion (e.g. that the ions "pull along" the electrons, constituting "ambipolar" diffusion).

As stated in section II. 2. 2, the energy equation of equations II. 28 can be solved immediately (assuming $K_n \propto T^*$) by reducing it to incompressible form with the Howarth transformation (Ref. 7). This determines T^* and η^* as functions of x^* and t^*, and therefore also $D_{en}(x^*, t^*)$. The remaining unknowns are N, n and E^* as determined by the three remaining equations. The solution exhibited in reference 7 is approximately locally incompressible. That is, the heat transfer at any point is approximately given by the solution to the simple heat equation with constant diffusivity given for local conditions. In particular, near the wall or far out in the gas where the temperature and density are specified by the boundary conditions, this approximation can be used. Using this idea, the equations for incompressible diffusion (II. 29) are assumed to be a sufficiently

accurate description near the wall if local temperature and density are used. Using the usual shock tube terminology in which $(\ )_5$ refers to conditions behind the reflected shock wave, the reference quantities (eq. II. 19) become

$$T_\infty = T_1 = 300^\circ K$$

$$\eta_\infty = \eta_5 \frac{T_5}{T_1}$$

$$n_\infty = n_5$$

$$\lambda_\infty = \left(\frac{\varepsilon_o k T_1}{e^2 n_5} \right)^{\frac{1}{2}}$$

$\left((D_{en})_\infty \right.$ based on T_1 and $\eta_5 \frac{T_5}{T_1}$, etc.$\left.\right)$ The order of magnitude of these quantities is exhibited in Table I. Note that for computing, say, the fluxes of charged particles near the wall, one uses transport parameters evaluated at room temperature. These quantities are, of course, well known, in contrast to those for $T_5 \sim 10,000^\circ K$.

From Table I it is seen that the characteristic time γ (eq. I. 19) $\sim 10^{-9}$ seconds. On the other hand, in the shock tube a typical unit of time is 10 μ secs. Thus our main interest centers around large time, i.e. $t^* = O\left(\frac{1}{D}\right)$ or larger. The equations II. 29 will be discussed first for small time and then for large.

IV. 2 Diffusion for time $t^* = O(1)$

The boundary conditions for small time are not known *a priori* and the discussion of appendix III is of little use since it is largely for equilibrium. From section III. 3. 1, however, we do know that for the cold wall $n(0)$, $N(0) < 1$. Customarily the approximation is made that

$$n(0) = N(0) = 0 \qquad \text{(IV. 1)}$$

This assumption is used here to illustrate its implications.

A qualitative argument is first made to illustrate the features of diffusion for small time and then an expansion procedure is indicated which can be used to make a more thorough analysis. Equations II. 29 are non-linear partial differential equations with a small parameter D multiplying a highest order derivative, so that the expansion procedure will involve singular perturbations.

The small parameter D is the manifestation of the fact that ions diffuse much more slowly than electrons. The most important feature of the equations for small time is that initially $E^* = 0$, and the electrons and ions tend to diffuse independently. For a cold wall the large electron flux to the wall leaves a net plus charge in the gas. From equation II. 27 $E_t^* < 0$ so the field grows negatively. It exerts a force on the electrons away from the wall and on the ions toward the wall. However, to the extent that the approximate boundary condition $n(0) = N(0) = 0$ is correct, this force does not affect the fluxes at $x^* = 0$. The particles (at

least approximately) diffuse independently at $x^* = 0$ and the flux to the wall and the electric field at the wall ($E^*(0)$) are given by neglecting the body force terms. It is instructive to write down the relations for these quantities.

$$N_{t^*} - DN_{x^*x^*} = 0 \; ; \; N(0) = 0, \; N(\infty) = 1$$

(IV.2)

$$N = \operatorname{erf} \frac{x^*}{2\sqrt{Dt^*}}$$

$$n_{t^*} - n_{x^*x^*} = 0; \; n(0) = 0, \; n(\infty) = 1$$

(IV.3)

$$n = \operatorname{erf} \frac{x^*}{2\sqrt{t^*}}$$

$$E^*_{x^*} = N - n$$

(IV.4)

$$E^* = 2\sqrt{Dt^*} \; \operatorname{ierfc} \frac{x^*}{2\sqrt{Dt^*}} - 2\sqrt{t^*} \; \operatorname{ierfc} \frac{x^*}{2\sqrt{t^*}}$$

where $\operatorname{ierfc} x^* = \int_{x^*}^{\infty} \operatorname{erfc} \xi \, d\xi$, $\operatorname{erfc} x^* = 1 - \operatorname{erf} x^*$
and $\operatorname{ierfc}(0) = \frac{1}{\sqrt{\pi}}$. Therefore

$$F_i^*(0) = -D N_{x^*}(0) = -\frac{1}{\sqrt{\pi}}\sqrt{\frac{D}{t^*}}$$

$$F_e^*(0) = -n_{x^*}(0) = -\frac{1}{\sqrt{\pi}}\sqrt{\frac{1}{t^*}} \qquad \text{(IV.5)}$$

$$E^*(0) \doteq -\frac{2}{\sqrt{\pi}}\sqrt{t^*}$$

The field at the wall builds up with the square root of time and will continue to do so if $n(0) = N(0) = 0$. In particular, for large time

$$t^* = O\left(\frac{1}{D}\right) \Rightarrow E^*(0) = -O\left(\frac{1}{\sqrt{D}}\right) \sim -10 \qquad \text{(IV.6)}$$

It is evident that, in fact, the field can not continue to increase indefinitely. The only way to stop the increase of the field $E^*(0)$ is to relax the boundary condition III. 1. The understanding of the diffusion process for large time depends on obtaining a more accurate boundary condition at $x^* = 0$, even though the condition IV. 1 may be sufficient for small enough time.

A similar discussion applies for the solution at large distances from the wall. Since $E^*(\infty) = 0$ the particles also diffuse independently out near the edge of the advancing diffusion layer. Of course, as specified in section IV. 1, the reference quantities (eq. II. 19) are evaluated at conditions in the hot shocked gas. The first thing that happens at any large x^* is that the electrons start diffusing at $t^* \sim \frac{x^{2}*}{4}$. This serves to produce the field E^* which couples the two diffusion processes. As seen by equation IV. 4, the field attains a significant value at

$t^* \sim \frac{x^{2}*}{4}$. This point is completely missed in the "ambipolar diffusion" approximation of section II. 4.

IV. 2. 1. Expansion procedure for small time. The equations II. 29 can be expanded in terms of the small parameter D for times small enough that IV. 1 is valid. A boundary layer type solution for the ions will result. The first approximation for the outer solution is given by equations II. 29 with D = 0,

$$N_{t^*} = 0 \quad ; N = 1$$

while the first approximation to the inner solution is given by stretching the x-coordinate ($\tilde{x} = \frac{x^*}{\sqrt{D}}$) in the equations and then setting D = 0,

$$N_{t^*} - N_{\tilde{x}\,\tilde{x}} = 0$$

This is the same as equation IV. 2 so the ions are, to a first approximation diffusing independently. From these considerations we try the composite expansion

$$N(x^*, t^*) = 1 + \sqrt{D}\, N_1^{o}(x^*, t^*) + \ldots - \operatorname{erfc} \frac{x^*}{2\sqrt{Dt^*}} \left[1 + \sqrt{D}\, N_1^{i}(x^*, t^*) + \ldots \right] \quad \text{(IV. 7)}$$

where $(\ )^{o,i}$ refers to outer and inner respectively. Similarly,

$$n = n_o^{o} + \sqrt{D}\, n_1^{o} + \ldots - \operatorname{erfc} \frac{x^*}{2\sqrt{Dt^*}} \left[1 + \sqrt{D}\, n_1^{i} + \ldots \right]$$

$$E^* = E_o^{o} + \sqrt{D}\, E_1^{o} + \ldots - \operatorname{erfc} \frac{x^*}{2\sqrt{Dt^*}} \left[1 + \sqrt{D}\, E_1^{i} + \ldots \right] \quad \text{(IV. 8)}$$

Substituting these expansions into equation II. 29 and boundary conditions IV. 1 and equating terms of equal order gives

$$N = 1 + D\,N_2^{\,o} + \ldots - \operatorname{erfc}\frac{x^*}{2\sqrt{Dt^*}}\left[1 + \sqrt{D}\;N_1^{\,i} + \ldots\right]$$

$$n = n_o^{\,o} + \sqrt{D}\;n_1^{\,o} + \ldots - \operatorname{erfc}\frac{x^*}{2\sqrt{Dt^*}}\left[D^{3/2}\,n_3^{\,i} + \ldots\right] \qquad \text{(IV. 9)}$$

$$E^* = E_o^{\,o} + \sqrt{D}\;E_1^{\,o} + D\,E_2^{\,o} + \ldots - \operatorname{erfc}\frac{x^*}{2\sqrt{Dt^*}}\left[-2\sqrt{Dt^*} + D\,E_2^{\,i} + \ldots\right]$$

where

$$\left.\begin{aligned} &1)\ E_o^{\,o}{}_{t^*} - E_o^{\,o}{}_{x^*x^*} + E_o^{\,o}\,(1 - E_o^{\,o}{}_{x^*}) = 0;\ E_o^{\,o}(\infty) = 0,\ E_o^{\,o}{}_x(0) = 1 \\ &2)\ n_o^{\,o} = 1 - E_o^{\,o}{}_{x^*} \end{aligned}\right\}$$

$$\left.\begin{aligned} &3)\ E_1^{\,o}{}_{t^*} - E_1^{\,o}{}_{x^*x^*} + E_1^{\,o}{}_{x^*}E_o^{\,o} - E_1^{\,o}\,n_o^{\,o} = 0;\ E_1^{\,o}(\infty) = 0;\ E_1^{\,o}{}_{x^*}(0) = 0 \\ &4)\ n_1^{\,o} = -E_1^{\,o}{}_{x^*} \end{aligned}\right\}$$

$$5)\ N_2^{\,o}{}_{t^*} = -E_o^{\,o}{}_{x^*}\ ;\ N_2^{\,o}(\infty) = 0$$

$$6)\ E_2^{\,o}{}_{x^*} = N_2^{\,o} - n_2^{\,o}\ ;\ E_2^{\,o}(\infty) = 0 \qquad \text{(IV. 10)}$$

$$7)\ N_1^{\,i}{}_{t^*} = \frac{1}{2\sqrt{t^*}}\,E_o^{\,o};\ N_1^{\,i}(0) = 0$$

$$8)\ E_2^{\,i} = 2\sqrt{t^*}\;N_1^{\,i}$$

$$9)\ N_2^{\,i}{}_{t^*} = n_o^{\,o} - E_o^{\,o}{}_{x^*} - \frac{1}{2\sqrt{t^*}}\,(E_1^{\,o} + N_1^{\,i}E_o^{\,o} + 2\,N_1^{\,i}{}_{x^*});\ N_2^{\,i}(0) = N_2^{\,o}(0)$$

$$10)\ n_3^{\,i} = \frac{4\,t^{*\,3/2}}{x^*}\;n_o^{\,o}$$

The solution to the non-linear equation 1) is the key to the completion of the expansion IV. 9. All subsequent equations are, at worst, linear with variable coefficients. Equations 1) and 2) can be called the "frozen ion approximation" since they are obtained from equations II. 29 by setting $D = 0$. The solution is pursued no further here. It is simply pointed out that a numerical integration of equations 1) to 10) would of course yield a solution for small time to whatever accuracy desired, providing the accuracy of IV. 1 were no worse.

IV. 3 Diffusion for large time

The properties of equations II. 29 for large time can be exhibited by shrinking the time coordinate t^* by the small parameter D; $\tilde{t} = Dt^*$. The equations then become

$$N_{\tilde{t}} = N_{x^*x^*} - (NE)_{x^*}$$

$$Dn_{\tilde{t}} = n_{x^*x^*} + (nE)_{x^*} \qquad \text{(IV. 11)}$$

$$E_{x^*} = N - n$$

This stretching is non-uniform for large x^* since by equation IV. 2 .f. f. large x^* corresponds to small time.

The first striking fact to be noticed is that the small parameter D now appears in such a way that there is no singular perturbation. There is no longer a boundary layer of ion diffusion. Both electron and ion diffusion are of the same order.

The zeroth order approximation (D = 0) to these equations demonstrates the true meaning of the statement of section III. 1 that the ions "pull along" the electrons. In this case the electron equation can be integrated as in section II. 3 to give

$$n\,(x^*,\ \tilde{t}) \;=\; e^{\,V^*\,(x^*,\ \tilde{t})} \qquad \text{(IV. 12)}$$

To a first approximation the electrons are in isothermal equilibrium at each instant of time. This is the direct result of the tendency of the electrons to diffuse faster than the ions. In a coordinate system in which the ion diffusion is of O (1), the electrons appear to be in equilibrium at every instant. Equation IV. 12 states that the electrons are "pulled along" by the field which, in turn, is caused by both electronic and ionic diffusion. It is immediately seen that the assumption that $n = N$ in section II. 4 for ambipolar diffusion is much stronger than this statement.

The transformed continuity equation for electrons is

$$D\, n_{\tilde{t}} + F^*_{ex^*} \;=\; 0 \qquad \text{(IV. 13)}$$

so that the zeroth approximation gives $F^*_e = 0$. There is approximate equilibrium between pressure and body forces resulting in zero net flux. More precisely $F^*_e = O(D)$ and $n = e^{V^*} + O(D)$.

The complete expansion of equations IV. 11 in terms of

D yields little more information than that exhibited by the first approximation, because the equations remain non-linear to all approximations.

IV.3.1. Boundary conditions. Since the electrons are in equilibrium to order D, boundary conditions derived from equilibrium considerations, (section III.2.1) will be applicable to order D. If it is assumed that thermionic emission is the major source of electron flux from the wall, equation III.4a sets the boundary condition;

$$n(0) \doteq 4\sqrt{2\, n_\infty \lambda_\infty^3 \left(\frac{\lambda_\infty}{a_o}\right)^3}\; e^{-\phi^*} \qquad \text{(IV.14)}$$

or, using equation IV.12

$$V_o^* \doteq -\left(\phi^* - \ln 4\sqrt{2\, n_\infty \lambda_\infty^3 \left(\frac{\lambda_\infty}{a_o}\right)^3}\right) \qquad \text{(IV.15)}$$

Using the representative values from Table I and taking $\phi = 4.0$ V leads to $n(0) \sim 2 \times 10^{-57} + O(D)$ and $V_o^* \doteq -130 + O(\ln D)$. Evidently there is some other emission process which will give larger $n(0)$ and therefore a more realistic boundary condition, but this extreme case serves to illustrate that practically any process will give a number density $n(0)$ less than $O(D)$, the inherent inaccuracy of the method. This leads to a voltage quite insensitive to the error. For example, even in this case where $n(0)$ is fantastically small, the voltage at the wall is only $V(0) = -3.4$ V. The reason for this insensitivity is easily seen to be

due to the Boltzmann factor which enters all formulae such as IV. 14 and IV. 12 and which contains the temperature. For room temperature this multiplies the voltages in the exponentials by 39 causing these terms to be the determining factors for orders of magnitude.

In actual fact, the major source of electrons at the wall is probably photoemission by radiation from the ionizing gas. In the initial stages of ionization it will be largely resonance radiation. The number of excitations per unit volume and time can be estimated from reference 9, equation 11. The radiation emitted by these excited atoms must pass through a cold dense layer of thickness $\delta_5 \doteq \frac{2}{\sqrt{\pi \, Pr_5}} \sqrt{\nu_5 \, t}$ (Eq. 2) in which the radiation decays as $exp\left(\frac{-\delta_5}{L}\right)$ where L is the mean free path for radiation. It is assumed that the photons are emitted from a volume of one unit area cross section and one radiation free path thick. Thus for F_p, the flux of photons striking unit area of the wall, we have

$$F_p \doteq L \eta_5^2 \, S_* \, \bar{c}_n \left(\frac{e\theta}{kT} + 1\right) e^{\frac{-e\theta}{kT}} \, e^{-\frac{\delta_5}{L}} \qquad \text{(IV. 16)}$$

where S_* is the cross section for excitation, $\bar{c}_n$ the mean thermal velocity of atoms in the hot gas, and θ the energy of the first excited state. From Table I and reference 9 we take $\eta_5 = 2 \times 10^{22}$, $\bar{c}_n = 2 \times 10^3$, $S_* = 10^{-21}$, $\theta = 11.5$ V., $\frac{kT_5}{e} = .83$ V., $\delta_5 \doteq 2 \times 10^{-3}$ and $L \doteq 10^{-4}$, the value in the hot gas. This maximum value for L will give a maximum value of F_p. The result is $F_p \doteq 2 \times 10^9$. If each of these photons produces an

electron on impact, equilibrium will be established when the Maxwell Boltzmann flux of electrons to the wall from the gas equals this photoelectric flux, i.e. when $n(0) = 2 \times 10^{-16}$. The voltage V_o^* appropriate to this is $V_o^* = -36$ or $V(0) = -.93$ volts.

Both processes discussed here have resulted in $n(0) \ll O(D)$ and $V(0) = O(1)$. Thus, to a first approximation (and, in fact for all approximations up to at least $O(D^6)$) there is little to choose from between these boundary conditions. In essence, the boundary condition $n(0) = 0$ has been relaxed only so far as required to maintain $V(0) = O(1)$, but may still be used to a good approximation when computing fluxes.

It still remains to determine the boundary condition $N(0)$ which in section III.3.1 was established to be $N(0) < 1$. It is evident that, because of the large ion mass, the ion diffusion is not greatly perturbed at large time though electron diffusion is (compare eq. II.35 for ambipolar diffusion with eq. IV.2 for free diffusion). Thus it seems that a valid approximation would still be $N(0) = 0$. With this boundary condition, free diffusion occurs near the wall just as for small time. From equation IV.5

$$F_i^*(0) \doteq -\frac{1}{\sqrt{\pi}} \sqrt{\frac{D}{t^*}}$$

so that for $t^* = \frac{\tilde{t}}{D}$, $F_i^*(0) = O(D)$, the same order as F_e^*. The electron flux has been reduced from $O(1)$ for small time to $O(D)$ for large time while the ion flux has reduced naturally from $O(\sqrt{D})$ to $O(D)$.

Since $F_e^*(0) \sim F_i^*(0) = O(D)$ then, from equation II.27,

$E_t^*(0) = O(D)$, a result consistent with equations IV. 14 and IV. 15 which are independent of time. The value of the electric field is given by equation IV. 6.

There is, in principle, a composite expansion equivalent to equation IV. 9 which would match the "inner" solution of equation II. 29 for small time with the "outer" solution of equation IV. 11 for large time. However, a set of boundary conditions applicable for all time must be expanded and used to obtain the composite solution as was done in section IV. 2. 1. It is the main point of section III. 1 that these complete boundary conditions are not known a priori and that, in fact, they have only been estimated for equilibrium with a metallic wall. Thus, it is felt that the approximate results exhibited in this section go as far as current knowledge allows and that the next step lies in a better understanding of general matching conditions at the interface between the wall and partially ionized gas.

It goes without saying that this limitation will arise any time there is an ionized gas in the neighborhood of a hot or cold wall whether or not there are other body forces or convective velocities to further complicate the equations.

The following conclusions about the diffusion process for large times can be made: 1) From the result II. 33 for equilibrium and the demonstration in section IV. 2 that the field near the wall is very sensitive to the boundary condition, it is concluded that the space charge effects for $x^* \prec 1$ ($x \prec \lambda_\infty$) are largely due to the presence and properties of the wall. The ambipolar diffusion approximation misses this point by maintaining the boundary conditions IV. 1 thus causing the field to become arbitrarily large

near $x = 0$ to maintain finite fluxes (eq. II. 36). On the other hand, the ambipolar diffusion result <u>for the fluxes</u> is consistent with the order of magnitude result of this section. However, it can not be established that equation II. 37 is a better approximation than the even simpler computation IV. 5 ($F^*_e(0) \sim F^*_i(0) \doteq \frac{1}{\sqrt{\pi}} \sqrt{\frac{D}{t^*}}$).

2) The free diffusion result for large x^* and the approximation in this section for boundary conditions at large time indicate that the conditions IV. 1 can be used in an approximate description of the space charge field for $x^* \gg 1$ resulting from the difference in fluxes between electrons and ions. For $x^* \gg 1$ the space charge effects are quite independent of the properties of the wall material. This is the idea behind the ambipolar diffusion approximation, but its strong assumption masks the "precursor" signal due to free electron diffusion (eq. IV. 3) which causes a field of order 1 at $\frac{x^*}{2\sqrt{t^*}} \doteq 1$ rather than at $\frac{x^*}{2\sqrt{2\ Dt^*}} \doteq 1$ as predicted by equation II. 35.

APPENDIX V

THE ROLE OF DIFFUSION AND IONIZATION IN THE SAMPLING EXPERIMENT

V.1 Introduction

In this appendix the experiments which were carried out to determine the utility of a molecular beam sampling device in the study of low density shock tube flows are described. The sampling consists of the extraction of a beam of particles from the shock tube through a small hole, similar to the way a standard molecular beam is drawn from a gaseous source. In the case of a steady molecular beam, if the process by which the beam is extracted is understood (i.e. Knudsen flow) then measured properties of the beam (e.g. velocity distribution) provide information on the properties of the gas in the source. The same is true in the case of the shock tube sampling device where the conditions in the "source" are functions of time.

The large amount of information that can be obtained from the study of directed beams of particles (as contrasted to material in bulk) has been proven by the many beam techniques used today in physics such as mass spectroscopy, nuclear resonance studies, etc. A particularly alluring property of directed beams for shock tube studies is that the molecules in the beam do not collide with one another after passing through the hole. Thus, any chemical reaction which takes place upstream of the hole is frozen into the beam and can be studied at leisure downstream. (This statement must be modified

for effusing charged particles where long range forces act and "collisions" do, in fact, occur.)

A most important point arises with the shock heated molecular beam source concerning the actual nature of the "source". For the case in which the hole diameter is much smaller than the mean free path of gas particles just upstream of the hole (Knudsen flow), the sampling is, on the average, from a region about one mean free path away from the hole. This fact becomes important if the properties of the gas are functions of distance from the hole as, for example, in any isothermal atmosphere where body forces (i.e. gravitational or centrifugal) are applied or in the shock tube where the wall is much colder than the shock heated gas.

In the latter case a thermal layer grows parabolically in time after the shock reflects from the end wall (secs. II. 1 and VI. 1). The gas is cooler and more dense near the wall than far away. The thermal layer grows to one mean free path thickness in one mean molecular collision time after reflection. (The collision time is also the characteristic time for the shock reflection process, so for times less than the mean collision time the shock reflection and the thermal layer growth are intermingled.) For times much larger than the mean collision time (the case for the present experiments) the reflected shock is far away from the wall and the thermal layer has a well-defined thickness of many mean free paths. Since a molecular beam effusing through a hole which is much smaller than the mean free path near the hole effectively samples the gas from a region one free path from the hole, the "source" of the beam in the shock tube experiments is necessarily inside the cool, dense thermal layer. The thermal

layer therefore plays an important role in the interpretation of the properties of the effusing beam. This was first pointed out to the author by Dr. A. Thomson and is discussed in section V. 2.

The main experimental difficulty lies in the detection of the particles and the measurement of the desired properties. Since the measurement of an electric current is one of the easiest and most flexible measurements possible, it was decided that the experiment to test the utility of the sampling device should simply consist of the measurement of the flux of charged particles through the hole. By this choice the experiment becomes a study of a chemical reaction; namely, the ionization of argon behind a reflected shock wave. Actually, the flux of ions and electrons through the hole depends on two processes: 1) their rate of production behind the shock wave, and 2) the manner in which they diffuse through the growing thermal layer. Neither of these processes is well understood at this time, so unambiguous conclusions from the experiment regarding one of them are impossible. However, as a result of the detailed investigation of the diffusion of charged particles in appendices II, III and IV, a reasonably sound model for the manner in which the particles get from the shock heated gas to the collecting electrodes downstream of the hole can be formulated and used to provide information about the ionization process. This model and the ionization process are discussed in the next two sections.

V. 2 The Effusion of Charged Particles from a Shock Heated Gas

We are concerned here with the case in which the amount of

material withdrawn from the source is so small that none of the gas upstream of the orifice is disturbed. The thermal layer forms as if there were no hole. In the case of a very large orifice or nozzle such as the customary shock tunnel in which continuum flow exists, the region near the nozzle is of course greatly affected by its presence. In this section the model for the small orifice is discussed and compared with the large orifice case when the flow in both is expanded to zero density, i.e. to a directed beam in which particles do not collide. Finally, the nature of the actual experiments, which fall between the two limiting cases, is discussed.

Appendices II, III and IV outline the details of the diffusion of charged particles from a region in which the number density of electrons and ions is a prescribed constant n_∞ to a cold wall. It is concluded that the flux of the particles to the wall can be approximated by the result of the ambipolar diffusion assumption (Sec. II.4) which written in dimensional notation is

$$n_i = n_e = n_\infty \operatorname{erf} \frac{x}{2\sqrt{2 D_{in} t}} \tag{V.1}$$

$$F(x = 0) = - n_\infty \sqrt{\frac{2 D_{in}}{\pi t}} \tag{V.2}$$

where D_{in} is the ionic diffusion coefficient evaluated at wall conditions (Sec. IV.1). Since in this approximation the equations are linear, the solution V.1 can be used as the fundamental solution to a small impulsive jump $dn_\infty(t^+)$ in the number density at infinity at time $t = t^+$ with boundary conditions $n_e(0) = n_i(0) = 0$,

$$n_{iFund.} = dn_{\infty}(t^+) \quad \text{erf} \quad \frac{x}{2\sqrt{2\, D_{in}(t - t^+)}} \tag{V.3}$$

and the general solution can be obtained by summing up all fundamental solutions,

$$n_i(x, t) = \int_o^t dn_{\infty}(t^+) \quad \text{erf} \quad \frac{x}{2\sqrt{2\, D_{in}(t - t^+)}}$$

$$= \int_o^t \frac{d\, n_{\infty}}{d\, t^+} \quad \text{erf} \quad \frac{x}{2\sqrt{2\, D_{in}(t - t^+)}} \quad d\, t^+$$

For the purpose of evaluating the integral we assume that the number density $n_{\infty}(t)$ obeys the law (eq. V.15),

$$n_{\infty}(t) = a\,(\eta,\ T)\ t^s$$

so that

$$n_i = a\, s \int_o^t t^{+s-1} \quad \text{erf} \quad \frac{x}{2\sqrt{2\, D_{in}(t - t^+)}} \quad d\, t^+ \tag{V.4}$$

and that the error function can be apprxomated by

$$\text{erf}\ \xi = \begin{cases} \frac{2}{\sqrt{\pi}}\ \xi & ;\quad 0 < \xi < \frac{\sqrt{\pi}}{2} \\ 1 & ;\quad \frac{\sqrt{\pi}}{2} < \xi < \infty \end{cases}$$

Then, defining a new variable of integration $\zeta = \frac{t^+}{t}$,

$$n_i \doteq \begin{cases} s\, n_\infty(t)\left[\dfrac{x}{\sqrt{2\pi D_{in} t}}\displaystyle\int_0^{1-\frac{x^2}{\pi D_{in} t}} \frac{\xi^{s-1}}{\sqrt{1-\xi}}\, d\xi + \int_{1-\frac{x^2}{\pi D_{in} t}}^{1} \xi^{s-1}\, d\xi\right] & ; \ \dfrac{x^2}{\pi D_{in} t} < 1 \\ n_\infty(t) & ; \ \dfrac{x^2}{\pi D_{in} t} > 1 \end{cases} \tag{V.5}$$

$$= \begin{cases} s\, n_\infty(t)\left[\dfrac{2x}{\sqrt{2\pi D_{in} t}} \displaystyle\sum_{\nu=0}^{s-1} \frac{(-1)^\nu}{2\nu+1} \frac{(s-1)!}{(s-1-\nu)!\,\nu!} \left\{1-\left(\frac{x}{\sqrt{\pi D_{in} t}}\right)^{2\nu+1}\right\} + \frac{1}{s}\left\{1-\left(1-\frac{x^2}{\pi D_{in} t}\right)^s\right\}\right] \\ n_\infty(t) \end{cases}$$

For the solution near the wall, $x / \sqrt{D_{in} t} \ll 1$ and,

$$n_i(x,t) \doteq n_\infty(t) \frac{2x}{\sqrt{2\pi D_{in} t}} \sum_{\nu=0}^{s-1} \frac{(-1)^\nu}{2\nu+1} \frac{s!}{(s-1-\nu)!\,\nu!} \quad ; \ \frac{x}{\sqrt{D_{in} t}} \ll 1$$

Finally

$$F_i(0,t) = D_{in}\left(\frac{\partial n_i}{\partial x}\right)_{x=0} \doteq n_\infty(t)\sqrt{\frac{2 D_{in}}{\pi t}} \sum_{\nu=0}^{s-1} \frac{(-1)^\nu}{2\nu+1} \frac{s!}{(s-1-\nu)!\,\nu!} \tag{V.6}$$

Equation V.6 gives the net flux of ions or electrons through a thermal layer to the cool wall containing an ionizing gas. The approximate boundary condition $n_e(x = 0) = n_i(x = 0) = 0$ implies that there is no flux from the wall to the gas (i.e. the contribution discussed in section IV.3.1 is negligible), so the wall is a perfect

sink to charged particles. Thus equation V.6 also gives the flux to the wall. A hole in the wall will not perturb the fluxes because it, too, is a perfect sink, providing it is small enough that a) the flux of neutral particles is so small that the thermal layer is not perturbed (diameter of the hole much smaller than the mean free path in the gas near the hole) and b) the perturbation of electric fields in the plasma due to the removal of a portion of the constant potential wall is small (diameter of the hole much smaller than the Debye length in the gas near the hole);

$$\text{dia.} \ll \Lambda_n$$

$$\text{dia.} \ll \lambda_\infty \tag{V.7}$$

where Λ_n is the mean free path for neutrals and λ_∞ is the Debye length (Eq. II.19) and where both are based on conditions near the wall (Sec. IV.1). Thus equation V.6 gives the flux of ions through a small hole.

The flux of neutral particles through the hole is given by the familiar Knudsen effusion formula based on conditions one mean free path from the wall

$$F_n(0) = \frac{\eta\,(\Lambda_n)\;\bar{c}_n\,(\Lambda_n)}{4}$$

For $\Lambda_n \frac{\partial \eta}{\partial n} \Big/ \eta \ll 1$, which is the case for reasonable times, then a Taylor series expansion leads to (cf. Eqs. III.6 and III.6a)

$$F_n(0) = \frac{\eta(0)\,\bar{c}_n(0)}{4} \qquad (V.8)$$

It is evident from V.8 that all particles that effuse through a small hole in the shock tube are first cooled to room temperature in the thermal layer. As a result, the effusing beam has a mean kinetic energy of about 1/40 e.v. This situation can be compared with the case in which a nozzle is used to expand to a free molecular beam, where the throat diameter d* is much larger than the mean free path in the stagnation chamber Λ_{no},

$$d^* >> \Lambda_{no} \qquad (V.9)$$

The flow in the nozzle is accelerated to much higher energies (of the order of the thermal energy in the stagnation chamber) before dissipative effects start to convert this kinetic energy back into thermal energy. The point at which most of the kinetic energy of the flow has been thermalized can be characterized in boundary layer terminology as the point at which the boundary layer has "filled" the nozzle. (For a cool conducting nozzle, as in the shock tube, this is also the point at which a significant fraction of the energy of the gas has been transferred to the wall.) A comparison of the point x_δ at which the boundary layer thickness δ equals d, the diameter of the nozzle, with the point x_Λ at which the mean free path $\Lambda = d$ will give a crude idea of whether or not a high energy free molecular beam can be generated in a nozzle. This is, of course, far over-stressing the boundary layer concept but should

give results of order of magnitude accuracy. It also neglects the thermalizing effect of any shocks that may exist in the flow.

For simplicity consider a power law nozzle, although the same general results apply for any duct. Then $d/d^* = 1 + (x/d^*)^n$ where d^* is the diameter at $x = 0$, the throat. Now the boundary layer thickness is given by $\delta \sim \sqrt{\frac{x\mu}{\rho u}}$ and the mean free path is $\Lambda \sim \frac{\mu}{\rho \bar{c}}$. The properties of state will be evaluated, for order of magnitude accuracy, at the wall where for a conducting wall the temperature T_w is constant and the density

$$\rho = \frac{p}{R T_w} = \rho_o \frac{T_o}{T_w} \left(\frac{d^*}{d}\right)^{2\gamma} \left(\frac{\gamma - 1}{2}\right)^{\gamma/2} \left(\frac{2}{\gamma + 1}\right)^{\frac{\gamma}{2}\frac{\gamma+1}{\gamma-1}}$$

The isentropic area-pressure relationship has been used in the last term with the assumption that the static pressure $p/po \ll 1$. An equilvalent simplifying assumption that the velocity u has reached its limiting value leads to

$$\frac{u}{\bar{c}_o} = \left(\frac{\pi \gamma}{4(\gamma - 1)}\right)^{\frac{1}{2}}$$

Then

$$\delta^2 \sim \times \Lambda_{no} \left(\frac{T_w}{T_o}\right)^{p+1} \left(\frac{d}{d^*}\right)^{2\gamma} \left(\frac{2}{\gamma-1}\right)^{\gamma/2} \left(\frac{\gamma+1}{2}\right)^{\frac{\gamma}{2}\frac{\gamma+1}{\gamma-1}} \left(\frac{4(\gamma-1)}{\pi\gamma}\right)^{1/2}$$

$$\Lambda_m \sim \Lambda_{no} \left(\frac{T_w}{T_o}\right)^{p+\frac{1}{2}} \left(\frac{d}{d^*}\right)^{2\gamma} \left(\frac{2}{\gamma-1}\right)^{\gamma/2} \left(\frac{\gamma+1}{2}\right)^{\frac{\gamma}{2}\frac{\gamma+1}{\gamma-1}}$$

where it is assumed that $\mu/\mu_o = \left(\frac{T_w}{T_o}\right)^p$

Setting $\delta = d$ gives

$$\frac{X_\delta}{d^*}\left(\frac{d_\delta}{d^*}\right)^{2(\gamma-1)} = \frac{d^*}{\Lambda_{no}}\left(\frac{T_o}{T_w}\right)^{p+1}\left(\frac{\gamma-1}{2}\right)^{\gamma/2}\left(\frac{2}{\gamma+1}\right)^{\frac{\gamma}{2}\frac{\gamma+1}{\gamma-1}}\left(\frac{\pi\gamma}{4(\gamma-1)}\right)^{1/2} \qquad (V.10)$$

and $\Lambda = d$ leads to

$$\left(\frac{d_\Lambda}{d^*}\right)^{2\gamma-1} = \frac{d^*}{\Lambda_{no}}\left(\frac{T_o}{T_w}\right)^{p+1/2}\left(\frac{\gamma-1}{2}\right)^{\gamma/2}\left(\frac{2}{\gamma+1}\right)^{\frac{\gamma}{2}\frac{\gamma+1}{\gamma-1}} \qquad (V.11)$$

For $x/d^* \gg 1$ then $\frac{d}{d^*} = \left(\frac{x}{d^*}\right)^n$ and

$$\frac{\left(\frac{X_\delta}{d^*}\right)^{1+2n(\gamma-1)}}{\left(\frac{X_\Lambda}{d^*}\right)^{n(2\gamma-1)}} = \sqrt{\frac{T_o}{T_w}\,\frac{\pi\gamma}{4(\gamma-1)}} \qquad (V.12)$$

If the nozzle is conical (n = 1) and $\gamma = 5/3$, then for a typical shock tube temperature ratio of $T_o/T_w \sim 30$, $x_\delta/x_\Lambda \sim 8$. For nozzles with $n < 1$ it will probably not be possible to get free molecule flow before dissipative effects have become significant. For $n > 1$, x_δ/x_Λ gets large, but in practice this advantage would be offset by such effects as separation and shock formation. In fact, in the limit $n \to \infty$ (a sharp edged orifice), most of the entropy increase is due to shock waves.

In summary, in the expansion through a small orifice to a free molecular beam, the gas is first cooled in the thermal layer and then sampled from a region one mean free path from the wall, while with a large nozzle the sample is drawn from the hot gas far away

from the wall and later "cooled" in the nozzle.

It can be seen from Table I that a typical experiment satisfies neither conditions V. 7 nor V. 9, but lies somewhere between. In this fact lies the major uncertainty in the interpretation of the experiments. The interior of the thermal layer is evidently very greatly perturbed by the mass flux through the hole, while toward its outer edge the effect is quite small. This fact is further discussed in section V. 5. 2.

A process which has been neglected above is recombination of electrons and ions within the thermal layer since no sink term was included in the original continuity equations of appendix II. (Recombination outside the thermal layer and at the wall can be accounted for in the boundary conditions n_∞ and $n_i(0)$ respectively.) An estimate of the relative importance of recombination rate is given by comparing $(\partial n/\partial t)_R = k_R n_\infty^2$ for recombination with $\partial n_\infty/\partial t$ from equation V. 20,

$$\frac{(\partial n/\partial t)\ R}{\partial n_\infty/\partial t} = \frac{k_R n_\infty t}{s} \qquad (V.13)$$

where k_R, the recombination coefficient, is evaluated near the wall. For the typical case in Table I, $k_R = 3 \times 10^{-13}$ (Ref. 16, p. 141), $n_\infty = 3.4 \times 10^{15}$ and $t = 2 \times 10^{-5}$ so

$$\frac{(\partial n/\partial t)R}{\partial n_\infty/\partial t} \sim 10^{-2}$$

For high pressures, say 150 μ, where n_∞ is as much as 15 times larger and k_R is larger, then recombination can have a large effect

on the flux through the layer. This is in fact the case and is discussed in section VI. 3.

As mentioned in section V. 1 above, the flow of the electrons and ions downstream of the orifice is not "free molecular" because of long range electrostatic forces. In fact, recombination will also occur in this region because of the attractive forces. The low densities insure that there will be no three body collisions, so the recombination energy will be released radiatively. The possibility of this process is eliminated in the present experiments by separating the charges immediately after they effuse through the hole.

V. 3 The Initial Stages of Ionization in Shock Heated Argon

The development of the ion density $n_\infty(t)$ upstream of the hole is comprised of the initial stages of ionization in the shock heated argon. This is indicated by comparing the expected equilibrium degree of ionization of .01 for a typical run (Table I, item 16) with the observed value of 10^{-7} at 20 microseconds as computed from equation V. 6 using figure 13 (Table I, item 20). Thus the experimental measurement of ion current consists of a direct observation of a small portion of the early stages of the relaxation process.

Previous investigators agree that the important ionizing reaction in the approach to equilibrium results from inelastic collisions of energetic electrons with atoms. The reaction rate is therefore proportional to $n_\infty \eta_\infty$, the product of the electron density and atom density (Eq. V. 15). Since the initial conditions in the shock heated gas are $n_\infty = 0$, some other reaction not involving electrons must initiate the ionization process. Petschek and Byron (Ref. 3) conclude that the

electron-atom reaction is dominant for degrees of ionization $\alpha > 10^{-3}$ but that some atom-atom reaction which they can not specify must account for the initial ionization.

A qualitative argument based on the properties of an electron-atom reaction serves to confirm that the present experiments do not, in fact, observe such a process. If it is agreed that the unit of time t (20 μ seconds) for the present experiments is much smaller than the time to reach equilibrium ionization t_{equil} (.01 sec., Table I, item 18), the exponential solution to equation V. 15 can be approximated as $\frac{n_\infty}{n_o} \doteq 1 + \frac{t}{t_{equil}}$ where n_o is some effective initial condition resulting from the initiating process. Thus in an electron-atom reaction the degree of ionization should increase linearly with time with a very small slope. As described below, the observed $n_\infty(t)$ is by no means linear. It is therefore concluded that an electron-atom reaction is not observed and that the present experiments observe a portion of the relaxation process in which only forward-going atom-atom reactions are important.

There are two general points of view as to the nature of these reactions. The one attributes the initial source of electrons to the ionization of "impurities" and the other invokes a series of argon-argon collisions. The term "impurity" here refers to a substance which would ionize faster due to collisions with argon atoms than argon itself, since otherwise the impurity process would not be observable. Therefore an impurity is a substance which has an ionization potential so much lower than argon's that, despite the low impurity concentration, more impurity ions are

produced than argon ions.

The first point of view receives its support from the result reported by Petschek and Byron (Ref. 3, Fig. 15) that the onset of total illumination behind a shock as indicated by a drum camera photograph is a function of impurity level. A somewhat more direct means reported by Alpher and White (Ref. 10) also gave qualitative dependence of relaxation time on impurity. (In both cases "Impurity" is not defined as above, but refers to all non-argon gases.) It has been inferred that impurity ionization is rate determining even though it may contribute a small fraction of the total equilibrium ionization. Thus the impurity reaction must be much slower than the final stage electron-atom ionization process but much faster than any alternative argon-argon initial ionization process.

The main proponent of the second point of view is Weymann (Ref. 9) who proposes a two step argon-argon process. Though this proposal does not account for the supposed dependence on impurity level and is probably an over-simplification of the actual process, it helps to fix ideas about some of the functional dependencies. For example, the two step process consisting of the excitation of an argon atom to the resonance state and the subsequent ionization of the excited atom gives the result (Ref. 9, Eq. 14)

$$n_{\infty} = 1/4\, \eta_{\infty}^{3}\, \bar{c}_{\infty}^{2}\, S^{2}\, t^{2} \left(\frac{E_*}{k T_{\infty}} + 1 \right) \left(\frac{E_+ - E_*}{k T_{\infty}} + 1 \right) \exp - \frac{E_+}{k T_{\infty}} \qquad (V.14)$$

where $\bar{c}_{\infty}^{2}$ is the mean atomic thermal velocity in the shock

heated gas, S a mean cross section for the total process, E_* the energy of the excited state (11.5 volts) and E_+ the ionization energy (15.76 volts).

Some general considerations in chemical kinetics illustrate the significance of the functional dependencies in this equation. The processes considered above such as impurity ionization, electron-atom ionization and recombination are simultaneous reactions (i.e. proceed simultaneously; c.f. Ref. 17, p. 1069). The initial stage of ionization is defined as the part of the total process in which only atom-atom forward-going reactions are important in the production of electrons. The electrons are produced in either one reaction or a series of consecutive reactions (Ref. 17, p. 1075). Any reaction which depends on the collision of two particles is a second order reaction since the rate depends on the product of two densities. The rate equation portrays the nature of a process as follows:

Consider a single second order reaction between species α and β producing ionized α. Then

$$\alpha + \beta \xrightarrow{k} \alpha^+ + \beta + e$$

and the rate equation is

$$\frac{dn_\infty}{dt} = k\, n_\alpha\, n_\beta \; ; \; \frac{n_\infty}{\eta_\infty} \ll 1 \qquad (V.15)$$

where n_α and n_β are the number densities of the reacting components, k is the rate constant and η_∞ the initial total number density. The inequality states that equation V.15 is valid

for the initial stages where η_∞ is essentially constant. The main feature of the rate constant is its familiar Arrhenius temperature behavior $\exp - E_a/k\,T$ where E_a is the activation energy for the reaction. Multiplying this Boltzmann factor is a weaker function of temperature often expressed in terms of a mean velocity and a reaction cross-section. If α is an argon atom then $E_a = E_+$.

For a consecutive series of first order reactions, say,

$$\alpha \xrightarrow{k_1} \beta \xrightarrow{k_2} \gamma^+ + e$$

it can easily be shown that in the initial stages (Ref. 17, p. 1075)

$$\frac{dn_\infty}{dt} = k_1 k_2 \eta_\infty \, t \qquad (V.16)$$

where, as before, $k_1 \sim \exp - E_1/kT$ and $k_2 \sim \exp E_2/kT$. Therefore $k_1 k_2 \sim \exp - (E_1 + E_2)\,kT$ and the total activation energy is the sum of the individual energies, $E_a = E_1 + E_2$. For argon $E_a = E_+$ as above.

Finally, for a consecutive series of second order reactions the integrated rate equation is similar to V. 14. From these three examples it can be seen that in general the density dependence in a rate equation comes from the order of the reactions, the time dependence comes from the number of consecutive reactions, while the activation energy is always the total energy for all steps.

The result is now applied to three possible ionizing reactions in argon. Weymann proposes the reaction

$$A + A \rightarrow A^* + A \rightarrow A^+ + A + e \qquad (V.17)$$

As stated above $E_1 = E_* = 11.5$, $E_2 = E_+ - E_* = 4.3$, $E_a = E_+ = 15.76$. If, on the other hand, an impurity I as defined above is present, then the reaction

$$A + I \rightarrow I^+ + A + e \qquad (V.18)$$

can proceed in any number of steps with the same result that the activation energy is the impurity ionization potential. In order to produce more electrons than an alternative argon reaction the impurity ionization potential must be so low that the increased Boltzmann factor more than accounts for the low impurity density in the rate equation. The most obvious substance with such a property is one of the alkali metals (e.g. sodium) whose ionization energies are about 5 volts; but the concentrations of alkali metal vapors in shock tubes must be extremely small.

Air is the major impurity in most shock tube experiments. The ionizing process in air that is thought to be most important is the consecutive series of reactions

$$O_2 + N_2 \rightarrow NO^+ + e + NO \qquad (V.19a)$$

with a total activation energy of 11.11 volts to produce one electron, or

$$O_2 + N_2 \rightarrow 2\,NO^+ + 2e \qquad (V.19b)$$

with a total activation energy of 20.36 volts to produce two electrons. It does not appear from these energies that air is a particularly

ionizable substance. For air impurity to contribute substantially to the argon ionization process, it must be present in amounts much larger than exp (11.11 - 15.76) $\sim$ 1 per cent. In these amounts it reduces the gas temperature behind a given strength shock sufficiently that the increased ionization rate is never observed for constant shock strength (c.f. Sec. IV.2.3). This is apparently in contradiction to the enhancement of the approach to equilibrium by air impurity observed by Petschek and Byron and Alpher and White.

V.3.1 Interpretation of experiments. For the interpretation of experiments the dependence discussed above can at least approximately be expressed as

$$n_\infty = \eta_\infty^{\,q}\ T_\infty^{\,r}\ t^{s}\ \exp\ (-E_+/k\,T_\infty) \qquad (V.20)$$

The constants q, r, s and E_+, determined from experiment, give information on the nature of the ionization process. The flux F of charged particles through an orifice depends on n_∞ and can be written

$$F = \eta_\infty^{\,q'}\ T_\infty^{\,r'}\ t^{s'}\ \exp\ -E_+/k\,T_\infty \qquad (V.21)$$

If equation V.6 describes the flux as a function of upstream conditions then $q' = q - 1/2$, $r' = r - 1/2$, $s' = s - 1/2$.

The derivative of the logarithm of the flux with respect to the inverse temperature gives the activation energy

$$\frac{\partial \ln F}{\partial\ 1/k\,T_\infty} = -(E_+ + r'\,k\,T_\infty) \qquad (V.22)$$

where usually, as indicated by V. 14, $r' < 0$. The second term on the right hand side, if r' is unknown, introduces an ambiguity in the experimental determination of E_+ which for the two step process V. 14 at the temperature considered here is less than 1 volt.

The slope of the flux vs. time on a log-log plot yields the "speed" of the reaction.

$$\frac{\partial \ln F}{\partial \ln t} = s' \qquad \text{(V. 23)}$$

As indicated by V. 14, the more steps in the reaction the slower the speed (the higher s'). For an n step process in the early stages $F \sim t^n$.

APPENDIX VI

EXPERIMENTAL RESULTS

VI. 1 Experimental Apparatus

The purpose of the apparatus is to measure the time history of the electric flux through the hole. Two electrodes, one biased positive for collecting electrons and the other biased negative for collecting ions, are placed immediately downstream of the hole as indicated schematically in figure 2. The electrons are duPont No. 4760 silver paint painted, baked, and polished on the top and bottom halves of the inside of a piece of 6 mm. glass tubing (3.6 mm. I.D.) 3.8 mm. long. A wire is connected to each half by soldering to baked silver paint on the outside diameter of the tubing and is lead out of the beam section through Amphenol hermetic seals. The electrodes subtend a solid angle of 43 degrees from the hole center line and therefore do not greatly block the flow of neutral particles. However, they are close enough to the hole that the time of flight from the hole to the downstream end of the electrodes for a beam of about 400m./sec mean velocity (room temperature) is less than 1 microsecond. Therefore, the uncertainty introduced by this time of flight in the time history of the shock heated gas is negligible. The leads from the electrodes are connected to mercury cell batteries E_1 and E_2 as shown in figure 2. The other pole of each cell is grounded either directly or across the .5 megohm input resistor of the pre-preamplifiers described in section I. 2. In the latter case, the signal from the amplifier, as recorded by the scope

comprises a time history of the current to the electrode.

The time origin, i.e. shock reflection time, can be determined by recording the output of the end wall thin film, heat transfer gauge (platinum on Scotch splicing tape, gauge No. 4, section I.3 f.f.) with one beam of the dual beam oscilloscope.

Other instrumentation for measuring shock strength and pressures is described in section I.2.

In all runs measuring electric flux, the following procedure is followed: After evacuation, the tube is flushed with argon and re-evacuated to the desired experimental pressure ($\sim$100 microns Hg.). The valve separating the beam and tube sections is then closed. Thereupon, the beam section pressure decreases rapidly until an equilibrium pressure ratio across the hole of about 500 (for a .32 mm. dia. hole) is established. The driver section is then pressurized with helium until the diaphragm breaks. As can be seen from Table I, the pressure in the shock tube rises by a factor of about 300 when the shock reflects from the end wall. Thus the total pressure ratio across the hole is about 10^5 during a run. The pressure rise in the beam section due to the additional mass flow during a run of 20 micro-seconds duration is $\Delta p/p \sim 3 \times 10^{-5}$, a negligible amount. The mean free path in the beam section during a shock tube run at $p_1 = 100$ microns is about 10 inches so true free molecule flow exists downstream of the hole.

VI.2 Preliminary Experiments

VI.2.1 Electrode bias. The mercury cells were chosen so that most of the charged particles that flowed through the hole were collected. This was accomplished experimentally by increasing the

the bias voltages E_1 and E_2 (Fig. 2) until the current to each electrode at a given shock strength and initial pressure was independent of bias. The result for the electron electrode was $E_1 = 2.6$ volts and for the ion electrode $E_2 = -5.4$ volts. Increasing both E_1 and E_2 by a factor of 3 caused no noticeable change in the current under given conditions.

The average ion passes in collision free flight from the hole along the axis between the electrodes with a kinetic energy of about 1/40 e.v. In order to trap this ion on an electrode, the voltage E_2 applied to the electrode must be such that (parabolic path)

$$\frac{\mathcal{E}}{E_2} < \left(\frac{\ell}{d}\right)^2 \qquad \text{(VI. 1)}$$

where $\mathcal{E}$ is the kinetic energy of the particle, ℓ the length of the electrodes along the axis and d the electrode separation. For the electrodes described above, $\ell/d \sim 1$ so relation VI. 1 is satisfied by the E_2 chosen.

The same argument applies to electrons. Since the mean velocity of the electrons is close to that of the ions (no charge separation), the mean electron kinetic energy is very much smaller. Equation VI. 1 therefore predicts $E_1 < E_2$.

The electron and ion currents were observed to be nearly equal at all times during the runs with E_1 and E_2 set as above. This result is consistent with the conclusion that there is little separation of charge for charged particles flowing through an orifice.

VI. 2. 2 Oscilloscope records of ion current and end wall gauge response. Figure 10 illustrates typical runs at three pressures in argon in which the current to the ion collector (upper trace) and the

end wall gauge response (lower trace) are recorded simultaneously. Figure 10a was recorded with compressed vertical and horizontal scales to illustrate the complete process. The increasing ion current is attributed to the growth of ionization in the shock heated gas while the subsequent decrease is due to quenching of this ionization.

The quenching can be due to cooling of the heated gas by, say an expansion wave or by the insulation of the heated gas from the hole by the growing thermal layer. The end wall gauge traces in figures 4 and 10 indicate the expected behavior for reflected and re-reflected shock waves in the absence of expansion waves, so the first possibility is ruled out. It is concluded that the cool, dense thermal layer provides a medium for recombination of electrons and ions as they migrate toward the wall. This conclusion indicates that even though the hole in these experiments is much larger than the mean free path at the wall and therefore greatly perturbs the interior of the cool layer, nevertheless the layer remains the major feature of the effusion process. As indicated in section V. 2 this result is expected for cases in which the hole diameter is smaller than or equal to the mean free path in the hot gas, $d^* \leq \Lambda_{on}$. Compare with condition V. 9 for continuum flow. On the strength of these indications, it is concluded that equation V. 6 is useable as an approximate representation of the flux of charged particles in the experiments considered here.

The end wall gauge identifies the beginning and end of a run by recording the shock reflection and the arrival of the re-reflected wave respectively. In figure 10a, which is merely an expanded version of figure 4c, the re-reflected shock arrives 20 μseconds

after shock reflection. Thus most of the ion current trace in figure 10a occurs after the run is over. In runs from which numerical data were obtained (e.g. Figs. 10 b and c) the current and time sensitivity were increased for better resolution of the increasing current.

VI. 2. 3 Introduction of impurities. Figure 11 compares a typical run in argon with three runs in which impurities were introduced. In figures 11b and c the tube was wrapped with heating tape and warmed to approximately 55°C. A test tube containing a few drops of mercury was attached to the shock tube at the flange for gauge No. 1 (Sec. I. 3) and was heated with a candle. The mercury partial pressure was probably more than 25 μ in addition to a measured argon initial pressure of 60 μ . Though the Mach number, computed for pure argon, has little significance, these traces exhibit graphically the ease with which mercury ionizes. Figure 11b shows a run with the same current and time sensitivity as in figure 11a, while trace c illustrates a similar run with the current scale reduced 1000 times! This large change in sensitivity with a flick of a switch emphasizes the flexibility of this simple experimental technique.

Several runs were made at an initial pressure of 95 μ of argon plus 5 μ of air to get a more quantitative indication of the effect of the largest source of impurity in these experiments. The amount of air added, however, was not sufficient to radically change the temperature in the reflected shock region. The ion current at 20 μ seconds fell on the experimental curve for $p_1 = 100\mu$ in figure 13 with a scatter similar to that shown in the figure. Thus the introduction of a few per cent of air does not affect the results of these experiments. This is consistent with the fact mentioned in

section V.3 that there is no known reaction in air that can be shown to be important in ionization. Of course, if there were some extremely effective reaction such that all of the ions observed were air-produced even in the highest purity runs, then the addition of air also would not give any significant change. The first alternative is certainly more realistic at the present time.

Addition of such large amounts of air that the reflected shock temperature decreased due to the change in γ and the total ionization potential increased because of reaction V.19, resulted in decreases of ion current as expected. At no time was air impurity observed to increase the ion current over the values observed in the experiments with the purest argon.

VI.3 Experimental Results

A determination of the time behavior of the ion current(s' in Eq. V.21) immediately gives some useful results about the effect of recombination in the cool layer on these experiments. It was found that replots of the oscilloscope traces on log log paper were straight lines for the first 20 μseconds or so and then became concave downward. The slope of the straight portion of the line is s' and is plotted in figure 12 as a function of Mach number and initial pressure. If recombination is important even in the first 20 μ seconds its effect will be to reduce s' . It is believed that this effect is observed in figure 12 at high pressure and Mach number. Under these conditions the density at the wall is higher and therefore k_R (Eq. V.13) is higher. Similarly n_∞ increases very strongly (factors of 50 in these experiments) with Mach number and pressure. Therefore equation V.13 indicates that recombination will be very

much more important (at a given time) at high temperature and pressure. Thus the maximum s' observed in these experiments can be considered a lower bound for the actual s' with no recombination. It is concluded that for this experiment s is at least 6.

The value of ion current on each trace at 20 μ seconds is plotted in figure 13 against the inverse temperature of the reflected shock region as computed from the measured Mach number assuming a perfect monatomic gas. The scatter in the data corresponds to, at worst, a scatter in temperature of 7 per cent. The slope of the dotted lines that have been fitted to the experimental data should give E_+ by equation V. 22. The decreasing slope with increasing pressure portrays the increasing effect of recombination in the thermal layer. The effect on ion current is larger at high Mach number so gives too small a slope; this effect gets larger with pressure. The effect of the term in r' in equation V. 22 tends to give a larger E_+ than the observed slope. In this experiment, where s' is so large, r' may also be large, say roughly -3, so E_+ may be a few volts larger than the observed slope. For $p_1 = 60\ \mu$ the experimental result is

$$\frac{\partial \ln F}{\partial\ 1/k\ T_\infty} = -12.6; \quad p_1 = 60\ \mu$$

Thus E_+ is at least 13 volts.

Finally, from figure 13 it is evident that the sensitivity to pressure (q') at a given Mach number and time decreases with increasing pressure. This effect would necessarily result if recombination were responsible for the behavior of s' and E_+

as proposed above. At M = 6.5 for the step between 60 μ and 100 μ , q' = 4.5 and, for 100 μ - 150 μ , q' = 1.6 so, extrapolating to $p_1 = 60$, it can be concluded that for this experiment $q' \sim 6$ at $p_1 = 60$.

These results indicate that the ionization process in the reflected shock region for $p_1 = 60$ at 20 μseconds (i.e. for degree of ionization $\alpha / \alpha_{equil} \sim 10^{-5}$) is a very slow process. A crude attempt to investigate this result further using the "local" reaction observed in the experiment can be made by arbitrarily generalizing Weymann's two step reaction to an s-step reaction. Then the unknown exponent r in equation V.20 is fixed and a more definite determination of E_+ results. In its generalized form equation V.14 is

$$n_\infty = \frac{1}{s!}\, n_\infty^{s+1} \left(\bar{c}_\infty\, t\, S\right)^s e^{-\frac{E_+}{k T_\infty}} \prod_{j=0}^{s-1} \left(\frac{E_{j,j+1}}{k T_\infty} + 1\right) \qquad \text{(VI. 2)}$$

where E_{ij} is the activation energy for the reaction from state i to state j. If, from the experimental results, s is taken as 6, then equation VI.2 predicts q = s + 1 = 7 and therefore $q' = 6\frac{1}{2}$ in fair agreement with experiment. At kT = 1 volt the product π in VI.2 gives $r \doteq -2\frac{1}{2}$ (assuming 6 equal steps in energy) and therefore $r' \sim -3$. Using this in equation V.22 gives $E_+ \sim 12.6 + 3.0 \sim 15.6$ volts in agreement with the expected 15.76 volts. This information can be used to finally solve equation

VI.2 for S, the mean cross section for all 6 steps for the typical run of Table I. This leads to $S \doteq 10^{-21}\ M^2 = 10^{-17}\ cm^2$, a reasonable number. This generalization is entirely arbitrary and has no physical justification aside from the very high experimental values of s' and q'. However it emphasizes the general conclusion that the reactions in the initial stages are much slower than previously suspected.

APPENDIX VII

SHORTING OF THIN FILM GAUGES

The shorting of thin film resistance gauges used for measuring heat transfer in shock tubes is now a familiar occurrence. It is well illustrated for a side wall gauge in figure 4a and for an end wall gauge in figure 10c. If the conductivity of the gas is such that a characteristic parallel resistance through the gas from one end of the gauge to the other changes the effective resistance of the gauge by an observable amount, then a "shorting effect" is observed. This effect would be a direct measure of the conductivity of the shock heated gas if conditions were uniform in the region near the gauge. However the analysis of charge diffusion to a cold wall in appendix IV indicates that the conductivity is by no means uniform near the wall. In fact from figure 3 it is obvious that the major contribution to the gas resistance will be very near the wall where the charge density is low. In fact for the boundary condition VI. 1 ($n_e(0) = n_i(0) = 0$), the conductivity from the hot gas to the wall is zero and no shorting is expected. A closer analysis of the shorting effect gives some information about the actual nature of the condition $n_{e,i}(0)$. A crude analysis is made in this appendix of the shorting of an end wall gauge.

The path of current in the shorting effect can be idealized as from one end of the thin film gauge through the thermal layer to the gas, through the gas (which is represented as a perfect conductor) parallel to the gauge and then back through the layer to the other end of the gauge. The effective resistance paralleling the thin film is $2r$ where

r is the resistance through the layer of a column of gas of cross sectional area, A/2 where A is the surface area of the film. Now

$$\frac{rA}{2} = \int_o^{\delta(t)} \frac{dx}{\sigma(x,\ t)} \qquad \text{(VII. 1)}$$

where $\sigma(x,\ t)$ is the local conductivity in mhos/m.

$$\sigma(x,\ t) = \frac{D_{en}\ e^2\ n_e(x,\ t)}{kT} \qquad \text{(VII. 2)}$$

From Table I it can be seen that the electron mobility $\frac{e\ D_{en}}{kT}$ is nearly constant throughout the thermal layer ($\doteq$ 60 near wall and $\doteq$ 90 in shock heated gas). We pick $\frac{e\ D_{en}}{kT} = 75$ and let

$$\sigma(x,\ t) = \sigma_\infty(t)\ \frac{n_e(x,\ t)}{n_\infty(t)} \qquad \text{(VII. 3)}$$

where therefore σ_∞ is independent of x. The integration of VII. 1 depends on the solution to the diffusion equations $n_e(x,\ t)$. We take in this crude argument the ambipolar diffusion result II. 35 but write it with non-zero boundary condition $n_e(0)$

$$n_e(x,\ t) = n_e(0)\left[1 + \frac{n_\infty(t) - n_e(0)}{n_e(0)}\ \operatorname{erf}\frac{x}{2\sqrt{2\ D_{in}\ t}}\right]$$

The integral in VII. 1 is evaluated approximately by representing the error function as in section V. 2. For $n_e(0) \ll n_\infty(t)$

$$\frac{n_e(x,\ t)}{n_\infty(t)} \doteq \frac{n_e(0)}{n_\infty(t)} + \frac{x}{\delta(t)} \quad ; \quad x < \delta \qquad \text{(VII. 4)}$$

$$= 1 \quad ; \quad x > \delta$$

Substitution of VII. 4 and VII. 3 into VII. 1 leads to

$$\frac{n_e(0)}{n_\infty(t)} = e^{\frac{-Ar\sigma_\infty}{2\delta}} \qquad \text{(VII. 5)}$$

The experimentally observed effect is a loss of signal $\Delta E/E$ as in figure 10c which, for a constant current gauge is $\Delta R/R$, where R is the resistance of the thin film gauge. This is related to the parallel resistance $2r$ by

$$2r = \frac{R}{\Delta R/R}$$

Finally, substituting this into VII. 5 gives

$$\frac{n_e(0)}{n_\infty(t)} = e^{\frac{-AR\,\sigma_\infty(t)}{4\delta(t)\frac{\Delta E}{E}}} \qquad \text{(VII. 6)}$$

As a numerical example data are taken from a typical run at $M = 6.5$ and $p_1 = 60$ (Run No. 747) giving $E = 2.35$ v., $R = 230\Omega$, $A = 1.5 \times 10^{-5}$. and ΔE at 20 μ seconds $\doteq .006$. From Table I, $\sigma_\infty = 4.1 \times 10^{-2}$ and $\delta(t) = 10^{-4}$, so

$$\frac{n_e(0)}{n_\infty(t)} \doteq e^{-33} \doteq 3 \times 10^{-15}$$

This simple crude calculation has provided a graphic experimental verification of the theoretical conclusion in section IV. 3. 1 that the boundary condition $\frac{n_e(0)}{n_\infty} = n(0) \ll O(D)$. It illustrates the

important conclusion that to make the diffusion process physically realistic the incorrect boundary condition $n_e(0) = 0$ need be relaxed only slightly. It also emphasizes that a "conductivity" measured in such a flow with cold probes is by no means the conductivity of the hot gas but is largely determined by the properties of the probe material (i.e. by the boundary condition $n_e(0)$)! The conductivity that is in fact measured is that of the part of the cool thermal layer immediately adjacent to the wall.

This analysis is of course only valid if the external measuring fields are smaller than the natural fields set up within the diffusion layer. In the case quoted above the field is $E/\delta \sim 10^4$ v/m. and the estimated natural field in equation III. 10 is $\sim 10^4$.

REFERENCES

1. Amdur, I. and Ross, J. "On the calculation of properties of gases at elevated temperatures." Combustion and Flame Vol. 2 (1958) pp. 412-420.

2. Hirschfelder, J.O., Curtiss, C.F., Bird, R.B. Molecular theory of gases and liquids, Wiley, N.Y. (1954).

3. Petschek, H. and Byron, S. "Approach to equilibrium ionization behind strong shock waves in argon." Annals of Physics Vol. 1 (1957) pp. 270-315.

4. White, D.R. "Influence of diaphragm opening time on shock tube flows." Journal of Fluid Mechanics Vol. 4 (1958) pp. 585-599.

5. Roshko, A. "On flow duration in low pressure shock tubes." To be published (Physics of Fluids).

6. Duff, R.E. "Shock tube performance at low initial pressures." The Physics of Fluids Vol. 2 (1959) pp. 207-216.

7. Roshko, A. "Heat transfer at the end wall of a shock tube" unpublished. For the original application of the same technique see Van Dyke, M.D. "Impulsive motion of an infinite plate in a viscous compressible fluid" Jour. App. Math. and Phys. (ZAMP) Vol. 3 (1952) pp. 343-353.

8. Fowler, R.H. Statistical Mechanics The University Press, Cambridge (1929).

9. Weymann, H.D. "On the mechanism of thermal ionization behind strong shock waves." Univ. of Maryland Institute for Fluid Dynamics and Applied Mathematics TN BN-144, July 1958.

10. Alpher, R.A. and White, D.R. "Optical refractivity of high temperature gases. II. Effects resulting from ionization of monatomic gases." The Physics of Fluids Vol. 2 (1959) pp. 162-169.

11. Rott, N. and Hartunian, R. "On the heat transfer to the walls of a shock tube." Cornell University Graduate School of Aeronautical Engineering, Nov. 1955.

12. Sommerfeld, A. Electrodynamics, Academic Press, N.Y. (1952).

13. Langmuir, I. "Adsorbed films of caesium on tungsten. Part I. The space charge sheath and image force." Phys. Rev. (1933) Vol. 43, pp. 224-251.

14. Guggenheim, E.A. Thermodynamics Interscience, N.Y. (1950), 2nd edition.

15. Fowler, R.H. and Guggenheim, E.A. Statistical Thermodynamics The University Press, Cambridge (1949), Chapter XI.

16. Von Engle, A. Ionized Gases The Clarendon Press, Oxford, (1955).

17. Glasstone, S. Textbook of Physical Chemistry, D. Van Nostrand, N.Y. (1946).

TABLE I

CONDITIONS BEHIND A REFLECTED SHOCK FOR A TYPICAL EXPERIMENT IN ARGON

MKSQ units unless otherwise specified

Given:

1) p_1 = 60 microns Hg = $.79 \times 10^{-4}$ atm. abs.
2) T_1 = $300^{\circ}K$
3) η_1 = 1.9×10^{21}
4) M = 6.5

Thermodynamic and transport parameters:

		in shocked gas		near wall	
		perfect gas	real gas	perfect gas	real gas
5)	T	9,600	8,100	300	300
6)	p	17.3 mm	17.0 mm	17.3 mm (1)	17.0 mm (1)
7)	η	1.7×10^{22}	2.0×10^{22}	5.6×10^{23}	5.4×10^{23}
8)	ρ	1.1×10^{-3}	1.3×10^{-3}	3.7×10^{-2}	3.6×10^{-2}
9)	μ	3.1×10^{-4} (2)	2.7×10^{-4} (2)	2.2×10^{-5} (3)	2.2×10^{-5} (3)
10)	ν	.28	.21	6.0×10^{-4}	6.1×10^{-4}
11)	D_{in}	.40 (2)	.31 (2)	8.1×10^{-4} (4)	8.2×10^{-4} (4)
12)	D_{en} (5)	77	59	1.5	1.6

(1) By assumption (section II. 2. 2)
(2) Ref. 1, Table 2, beam experiments
(3) Ref. 2, p. 562
(4) Ref. 2, p. 581
(5) Item 11 and Eq. II. 17

TABLE I (Con't)

	in shocked gas		near wall	
	perfect gas	real gas	perfect gas	real gas
13) K_n			1.76×10^5 (6)	1.76×10^5 (6)
14) Λ_n	3.8×10^{-4}		3.1×10^{-6}	
15) hole dia.			3.2×10^{-4}	

Parameters for equilibrium ionization:

16) $\alpha_{equil.}$		.012
17) $n_e = n_i$		2.4×10^{20}
18) t_{equil} (relaxation time)(7)		.015

Parameters of experiment at $t = 2 \times 10^{-5}$ sec:

19) n_∞ (8)	3.4×10^{15}	
20) α	2×10^{-7}	
21) λ_∞ (9)	1.2×10^{-4}	2.1×10^{-5}
22) γ (9)	1.8×10^{-10}	2.8×10^{-9}
23) δ (10)	2.2×10^{-3}	10^{-4}

---

(6) Ref. 2, p. 573
(7) Ref. 3, Fig. 15 converted for reflected shock region
(8) Figure 13 and Eq. V.6
(9) Eq. III.19
(10) Eq. 2

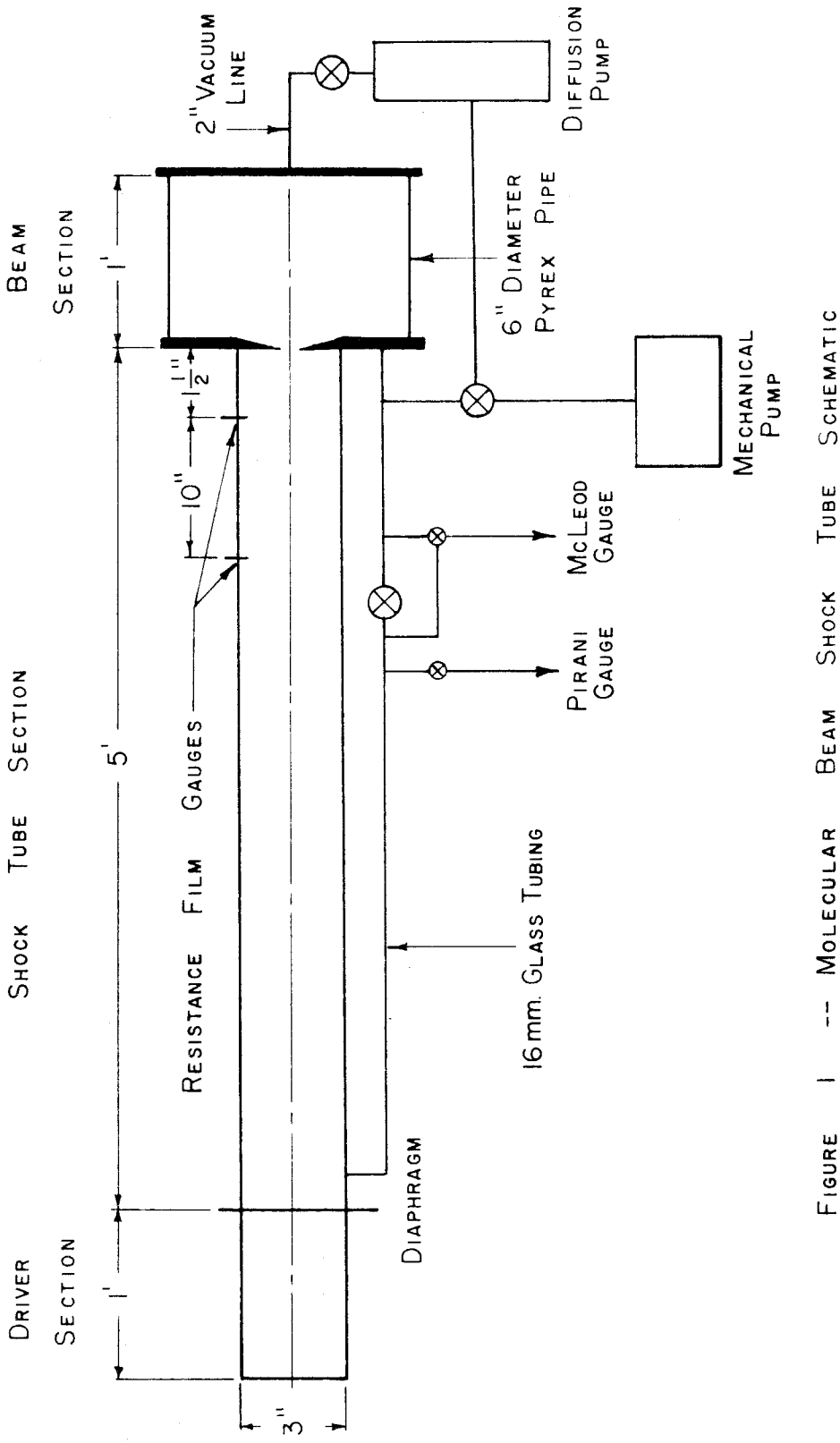

Figure 1 -- Molecular Beam Shock Tube Schematic

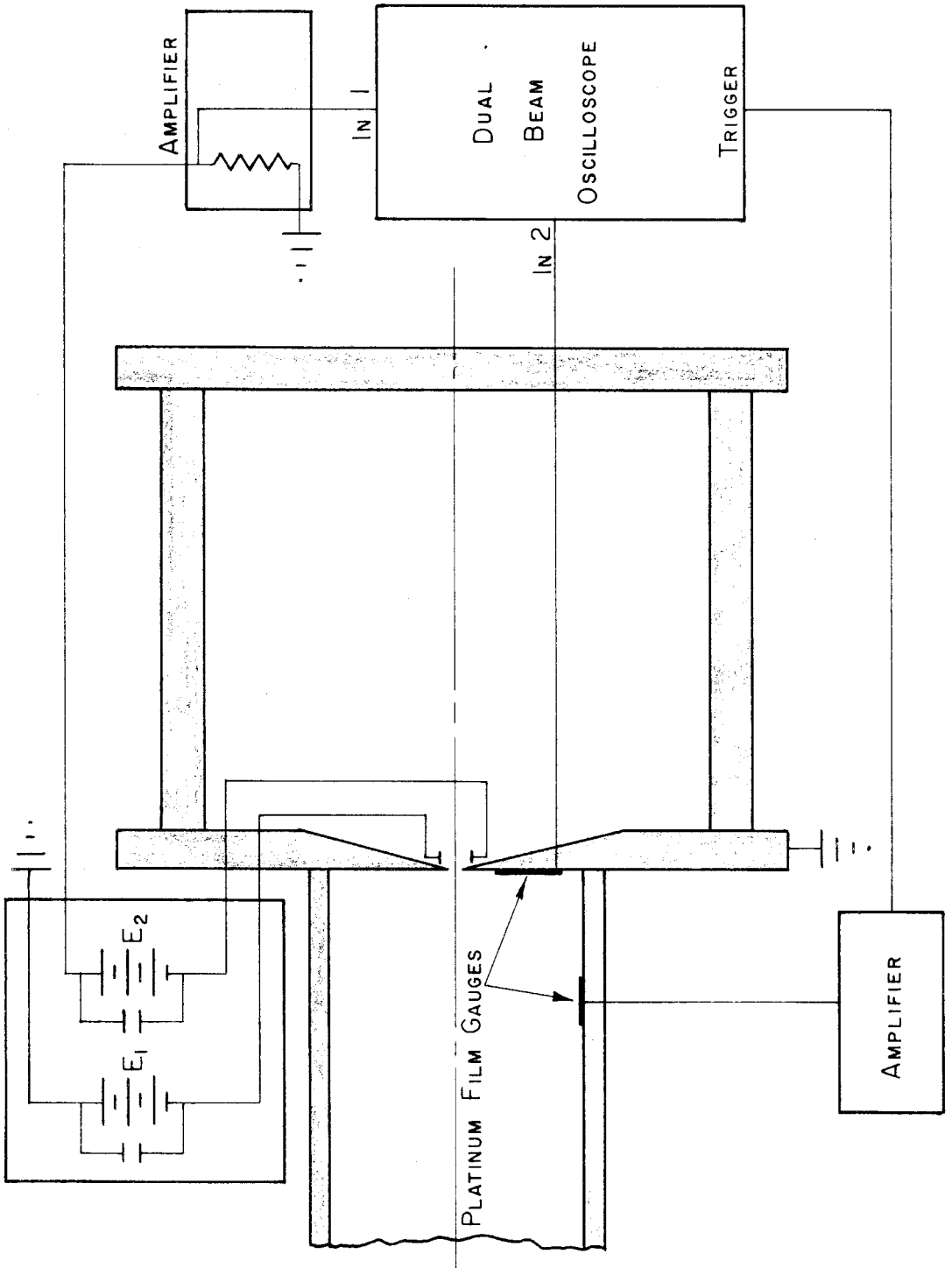

FIGURE 2 -- INSTRUMENTATION FOR IONIZATION EXPERIMENTS

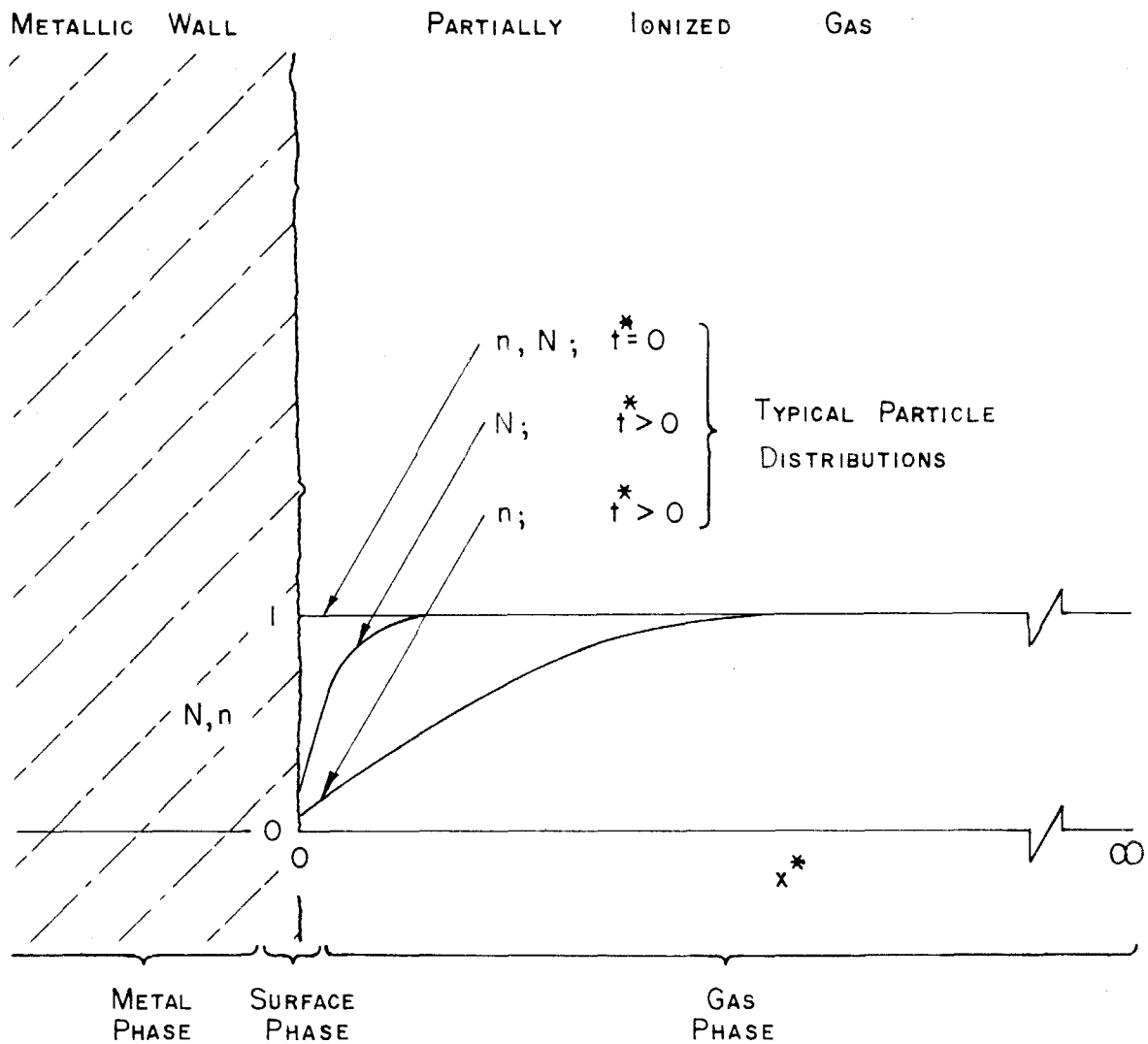

FIGURE 3 -- MODEL FOR CHARGE DIFFUSION PROCESS

Fig.	p_1 (mm)	M_{23}	gauge	sensitivity (volts/div.)	heating voltage	
4a	10	4.22	3	0.04	3.1	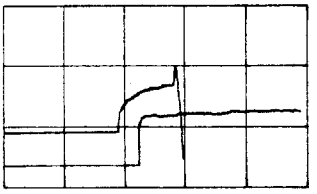 643
			4	0.04	1.05	
4b	1	5.8	3	0.04	3.1	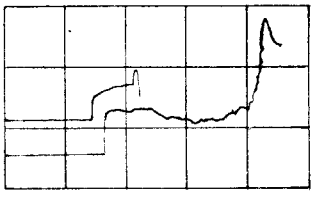 648
			4	0.04	1.05	
4c	0.1	6.55	3	0.02	3.1	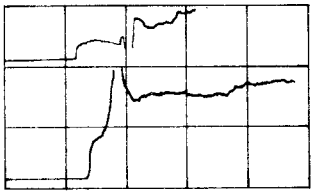 654
			4	0.02	1.05	

Figure 4. -- Side Wall (No. 3) and End Wall (No. 4) Film Signals Time plotted along abscissa (100 μseconds/division).

Fig.	p_1 (mm)	M_{23}	gauge	sensitivity (volts/div.)	heating voltage	
5a	10	4.38	1	0.02	1.25	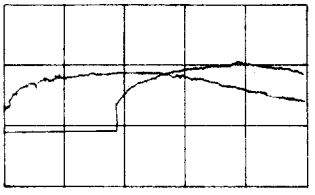 504
			2	0.02	1.25	
5b	1	5.75	2	0.02	1.25	 502
			3	0.02	1.25	
5c	0.1	6.75	2	0.004	1.25	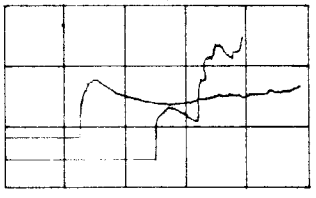 522
			3	0.004	1.25	
5d	0.01	7.30	2	0.001	2.25	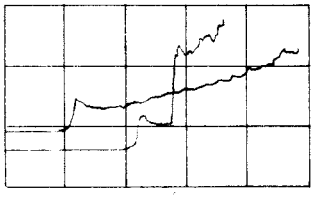 532
			3	0.001	2.25	

Figure 5. -- Side Wall Film Signals

Time plotted along abscissa (100 μseconds/division).

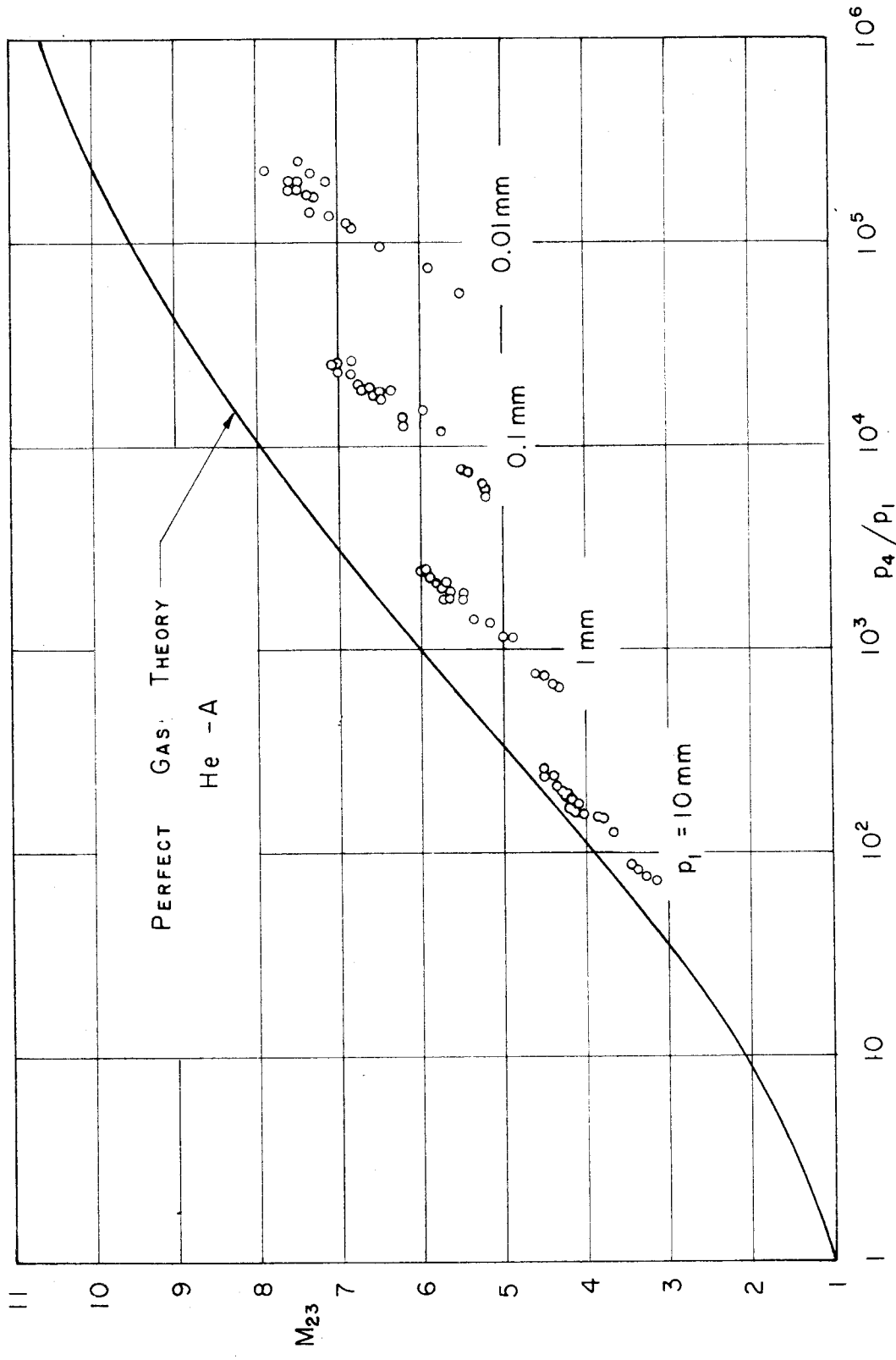

FIGURE 6 -- MACH NUMBER VS. DIAPHRAGM PRESSURE RATIO

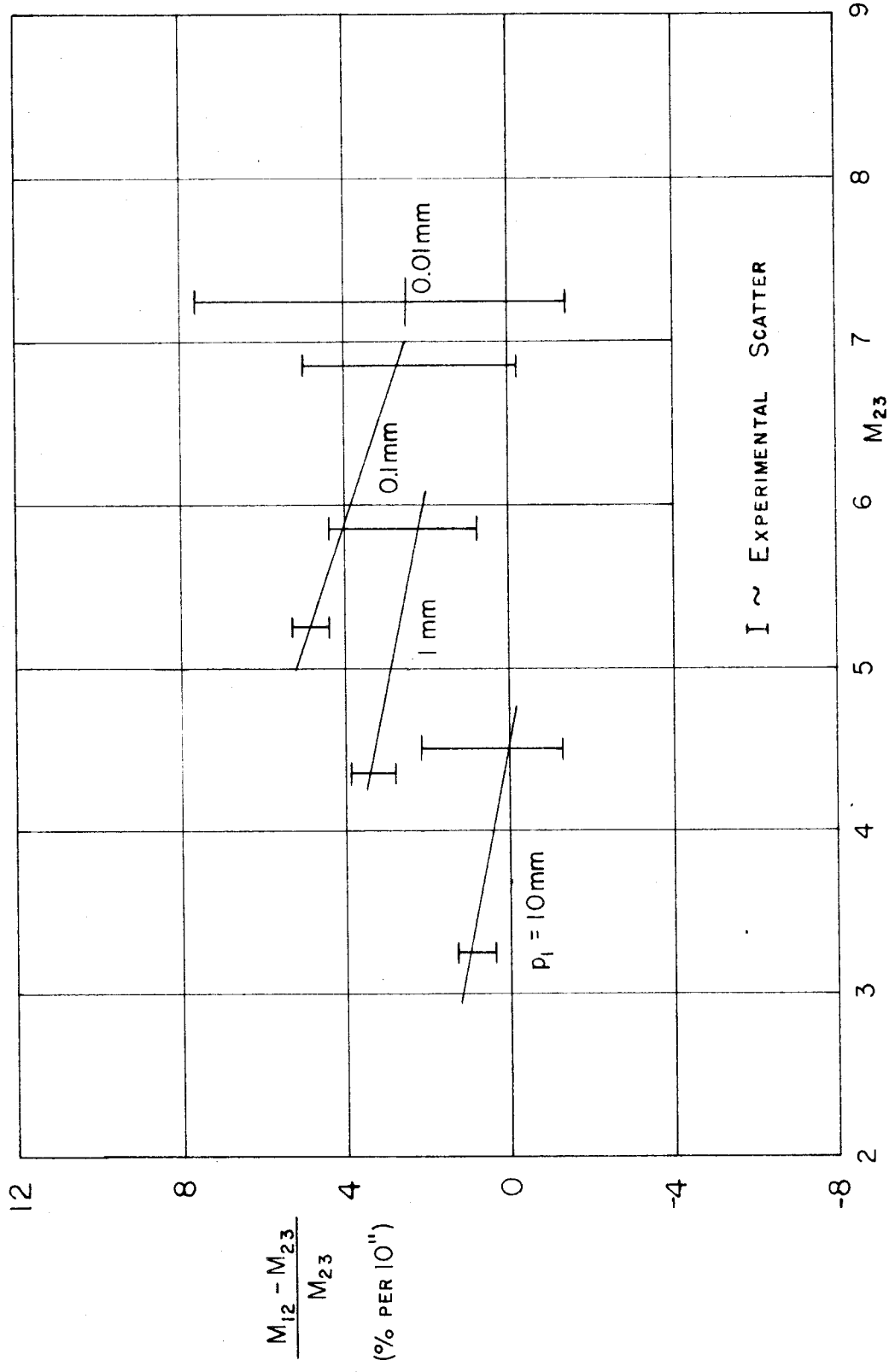

FIGURE 7 -- ATTENUATION BETWEEN TWO ADJACENT 10 INCH INTERVALS

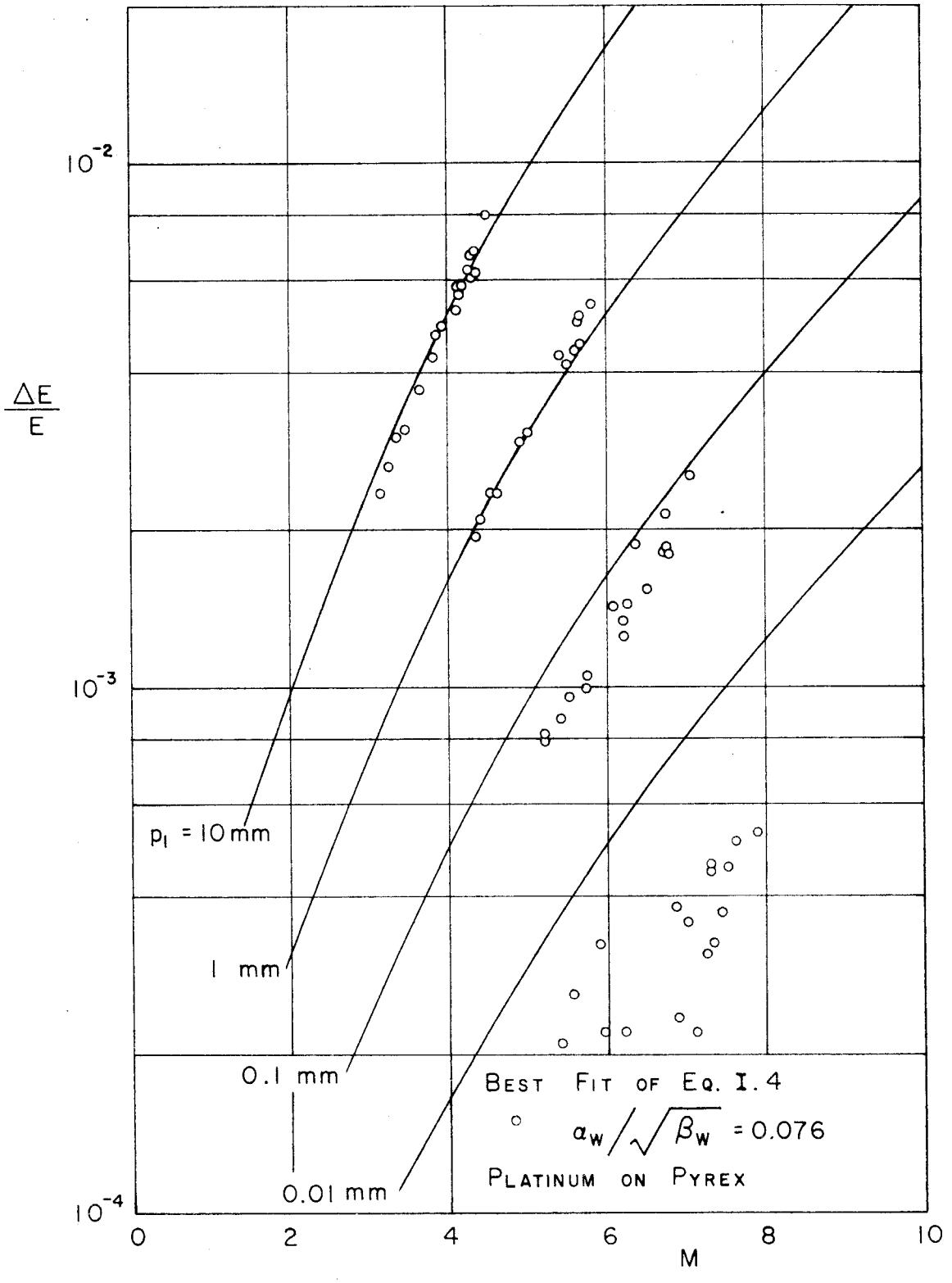

FIGURE 8 --HEAT TRANSFER TO SIDE WALL FILMS

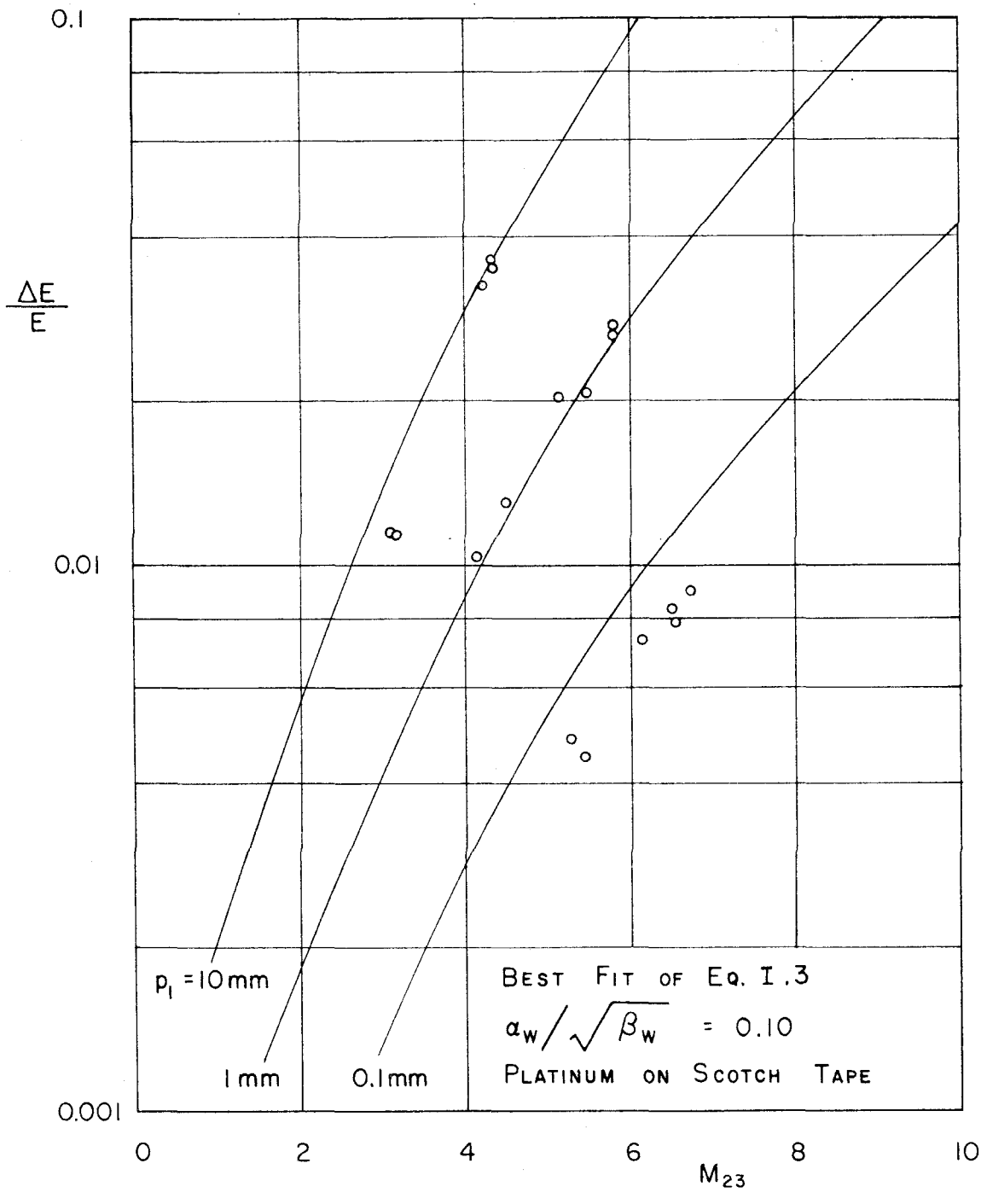

FIGURE 9 -- HEAT TRANSFER TO END WALL FILM

Fig.	p_1 (μ)	M	time (μsec./div.)	ion current (amps/div.)	
10a	60	6.65	20	4×10^{-9}	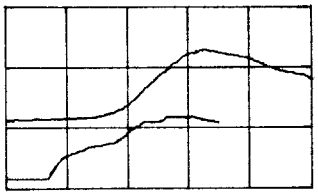 666
10b	100	6.55	10	2×10^{-9}	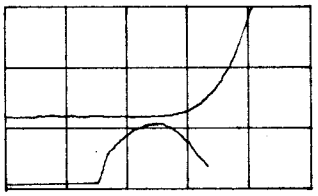 718
10c	150	6.55	10	2×10^{-9}	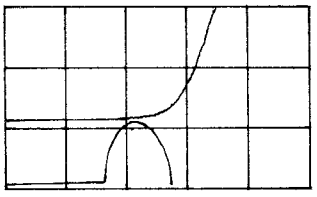 722

Figure 10 -- Simultaneous Ion Current (Upper Trace) and End Wall Gauge (Lower Trace) Signals

Fig.	p_1 (μ)	M	impurity	time (μsec./div.)	ion current (amps/div.)	
11a	60	7.0	argon	10	2×10^{-9}	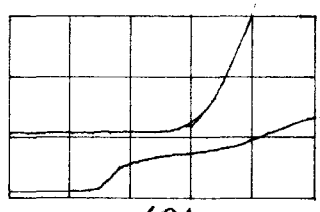 684
11b	60	6.9	Hg	10	2×10^{-9}	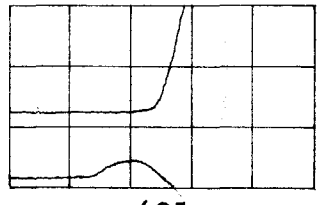 695
11c	60	6.7	Hg	20	2×10^{-6}	 707
11d	100	6.8	5% air	10	2×10^{-9}	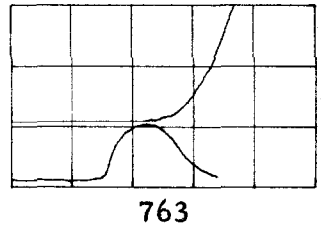 763

Figure 11 -- Effect of Impurities on Simultaneous Ion Current and End Wall Gauge Signals

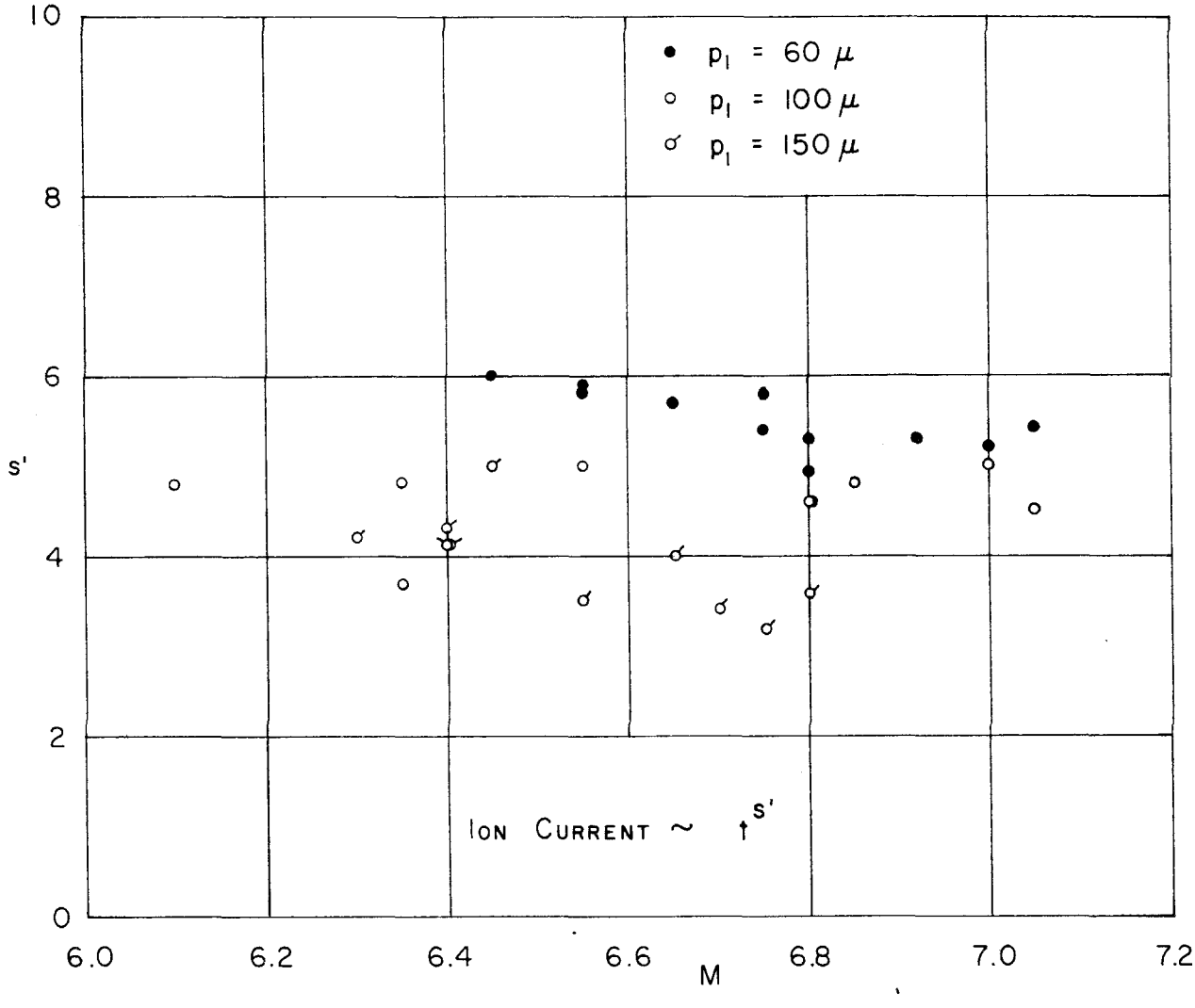

FIGURE 12 -- FUNCTIONAL DEPENDENCE OF ION CURRENT ON TIME FOR 20 μ SECONDS AFTER SHOCK REFLECTION

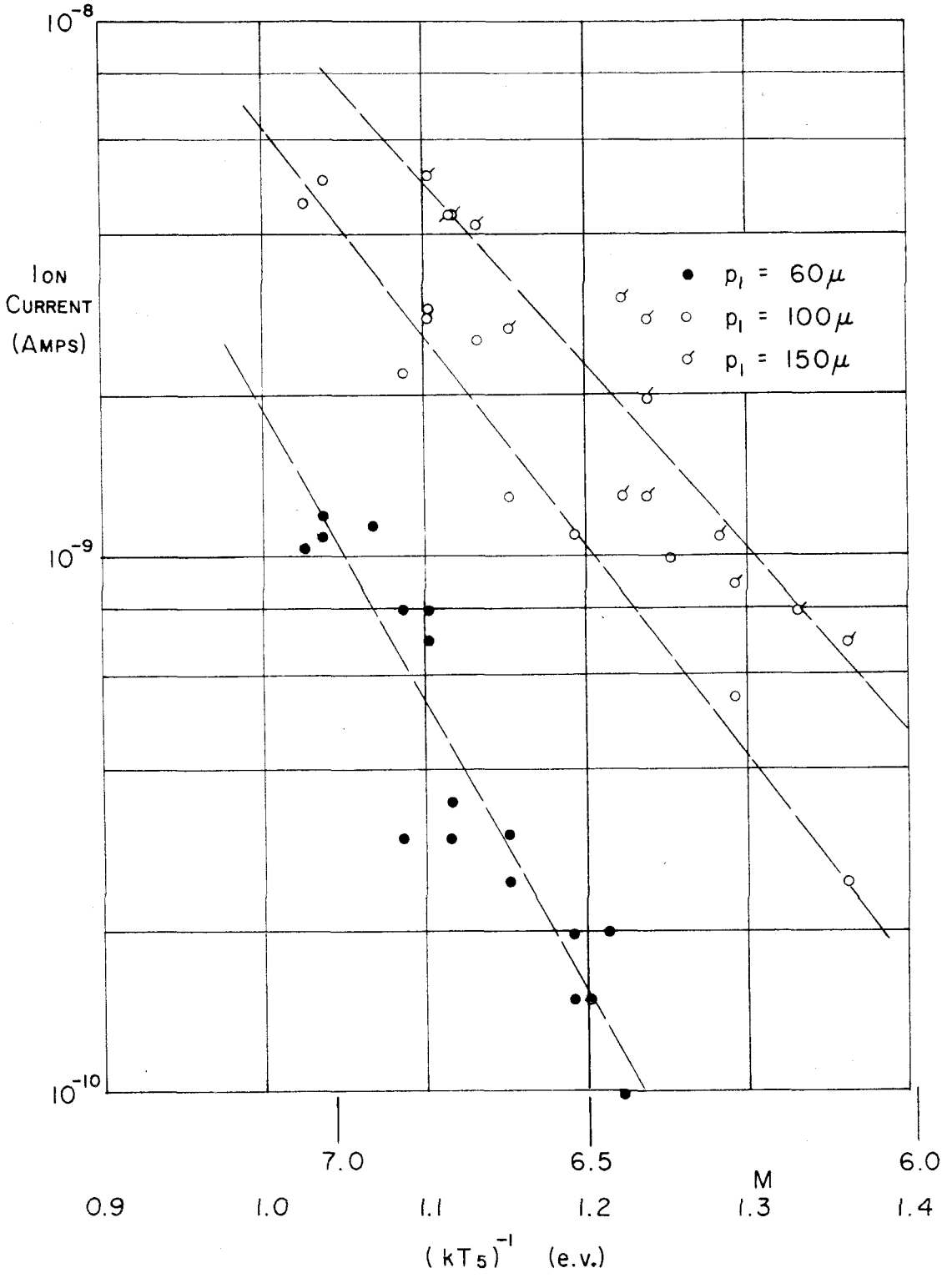

Figure 13 -- Ion Current at 20 μ Seconds after Shock Reflection vs. 1/kT Computed for Perfect Gas

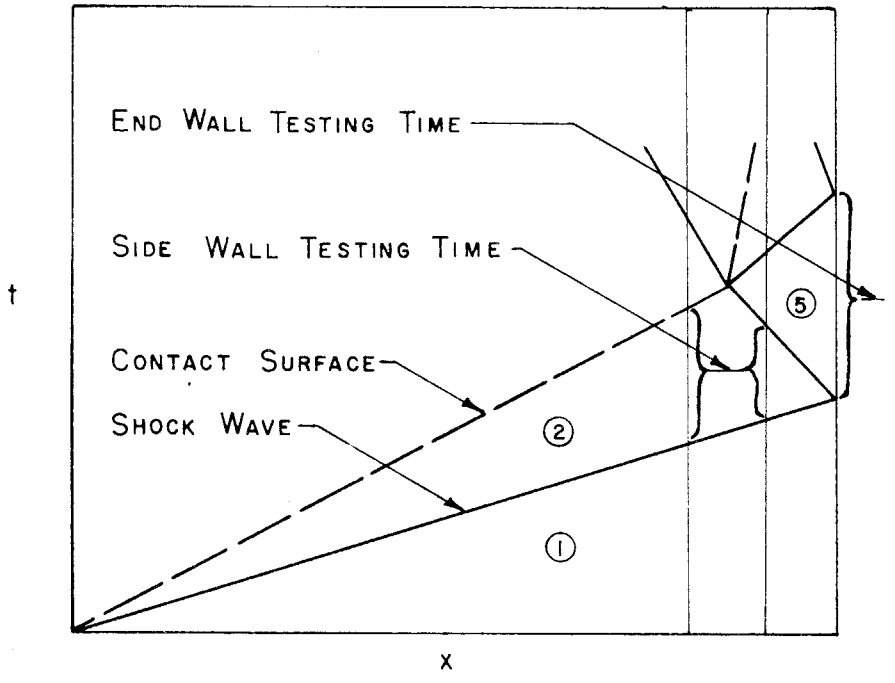

FIGURE 14 SCHEMATIC REPRESENTATION OF TESTING TIME FOR STRONG SHOCKS

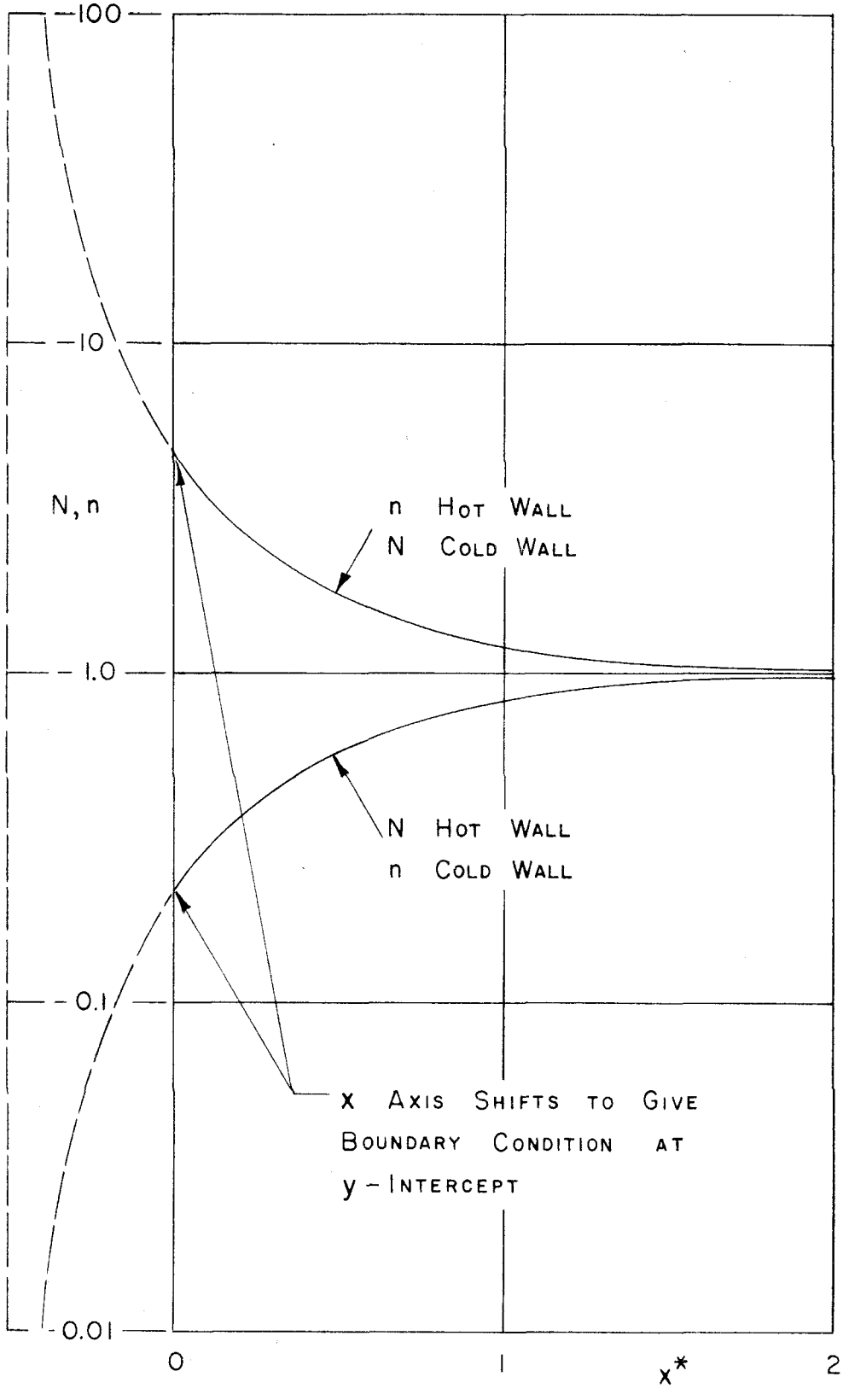

Figure 15 -- Isothermal Equilibrium (Eq. II.33)